NASA CONTRACTOR REPORT

THEORETICAL INVESTIGATION OF THE ABSORPTION AND SCATTERING CHARACTERISTICS OF SMALL PARTICLES

by N. L. Krascella

Prepared under Contract No. NASw-847 *by*
UNITED AIRCRAFT CORPORATION
East Hartford, Conn.
for

NATIONAL AERONAUTICS AND SPACE ADMINISTRATION • WASHINGTON, D. C. • APRIL 1965

THEORETICAL INVESTIGATION OF THE ABSORPTION AND SCATTERING CHARACTERISTICS OF SMALL PARTICLES

By N. L. Krascella

Prepared under Contract No. NASw-847 by
UNITED AIRCRAFT CORPORATION
East Hartford, Conn.

for

NATIONAL AERONAUTICS AND SPACE ADMINISTRATION

For sale by the Office of Technical Services, Department of Commerce,
Washington, D.C. 20230 -- Price $3.00

Theoretical Investigation of the Absorption and Scattering Characteristics of Small Particles

TABLE OF CONTENTS

Theoretical Investigation of the Absorption and Scattering Characteristics of Small Particles

SUMMARY

A theoretical investigation was conducted to determine the absorption, scattering, and extinction characteristics of small solid spherical particles which might be employed as seeding agents to control radiant heat transfer in gaseous nuclear rocket engines. The calculations were made using the Mie theory to determine the effect of particle size, wavelength, and particle temperature on particle opacity in those regions of the ultraviolet, visible, and infrared spectra for which complex index of refraction information was available. The following materials were considered: aluminum, carbon, cobalt, iridium, molybdenum, niobium, palladium, platinum, rhenium, rhodium, silicon, tantalum, titanium, tungsten, and vanadium.

INTRODUCTION

The absorption and scattering of electromagnetic radiation by small (0.01 μ to 1.0 μ radii) liquid or solid particles is of fundamental interest as well as being of interest in numerous practical radiation heat transfer problems involving advanced rocket concepts. For example, in various gaseous core nuclear rocket concepts (such as the concept of Ref. 1), energy is generated by nuclear fission in a central plasma core and transferred by thermal radiation to a surrounding propellant such as hydrogen. The propellant must be sufficiently opaque to permit absorption of this energy in the thrust chamber and to prevent damage of the rocket walls by excessive radiative heat transfer. However, hydrogen below a temperature of approximately 6000 K (10,800 R) at high pressure (1000 atm) is essentially transparent to thermal radiation (Ref. 2); thus, the need for "seeding" hydrogen propellant with opaque materials is evident at temperatures up to about 6000 K. Additional propellant opacity might be obtained by the addition to hydrogen of high melting- and boiling-point temperature solids or liquids in the form of small particles.

The spectral opacity characteristics of small solid carbon, hafnium carbide, aluminum oxide and tungsten particles dispersed in water (Ref. 3) and of small solid carbon and tungsten particles dispersed in nitrogen and helium (Ref. 4) have been experimentally measured. In addition, experiments have been conducted to determine the amount of energy which can be transferred by thermal radiation from a plasma heated by an electric arc to air seeded with carbon particles (Ref. 5). To date, however, no extensive theoretical analysis of the opacity of small absorbing particles for use as possible propellant seeding agents in the gaseous core nuclear rocket concept has been made. Such opacity calculations are required in order to permit the calculation of the radiative transfer of thermal energy to and through the seeded hydrogen propellant region.

The primary objective of the work described herein was the calculation of the theoretical extinction, absorption and scattering parameters of small particles using the Mie theory of Ref. 6.

CONCLUSIONS

1. There is no significant difference in the opacity of tungsten, rhenium and tantalum particles at a wavelength of 0.579 μ. (These three materials, of the fifteen materials investigated in this report, are of greatest interest for use as particle seeds in gaseous nuclear rocket engines because of their high boiling points (5565 to 5915 K or 10,017 to 10,647 R), high melting points (3270 to 3650 K or 5886 to 6570 R), and lack of reactivity with hydrogen).

2. Molybdenum, niobium, and iridium provide approximately the same opacity as tungsten, rhenium, and tantalum, but have melting points and boiling points approximately 500 K lower than those for tungsten, rhenium and tantalum.

3. Particles made of graphite and silicon have higher opacities than those made from any other materials investigated. However, these materials are not practical for use as seeds in gaseous nuclear rockets because carbon reacts readily with hydrogen and because silicon melts and boils at relatively low temperatures (1683 and 2890 K, respectively).

4. The opacity of solid tungsten particles is approximately independent of temperature.

5. The opacity of a particle per unit mass is approximately inversely proportional to the mass density of the particle or the atomic weight of the particle material.

EXTINCTION OF RADIATION BY SMALL PARTICLES

A pencil of electromagnetic radiation incident upon a material is, in general, attenuated; the totality of processes by which attenuation occurs being termed extinction (Refs. 7 and 8). In the present study, extinction is considered to consist of two processes, absorption and scattering. When the vibrating electromagnetic field of the incident beam impinges on the material, the electric charges within the body are forced to oscillate. The oscillations, however, are not strictly harmonic but are subject to resistive forces which dissipate a part of the incident energy in some other form such as heat. The dissipated energy no longer appears in the incident beam and is said to be absorbed. Those charges near the surface of the material reradiate a part of the energy which give rise to a reflected beam at some angle to the incident beam. Because the velocity of propagation of the energy within the medium is different from that in the surroundings, the incident beam is refracted (changes direction). For sufficiently small particles of material diffraction effects are also evidenced. The combination of reflection, refraction and diffraction give rise to scattered radiation.

The fractional decrease in the incident beam, I/I_0, due to absorption and scattering in a length, L, of material is given by:

$$I/I_0 = \exp\left[-L\,(\sigma_a + \sigma_s)N_i\right] \tag{1}$$

where I_0 is the incident intensity; I, the intensity after the beam traverses a length, L, of material; σ_a, the absorption cross-section; σ_s the scattering cross-section; and N_i, the number of absorbing and scattering centers.

The absorption and scattering cross-sections, σ_a and σ_s, are complex functions of the particle size, the wavelength of the radiation, and the refractive index of the particle (the refractive index is usually wavelength dependent). In general, the refractive index, N, may be mathematically expressed as:

$$N = n - ik \tag{2}$$

where n is the real part of the refractive index and k is the imaginary part. For bulk materials k is proportional to the absorption cross-section. In transparent materials k and hence σ_a are zero and no absorption occurs. The intensities of reflected and refracted waves are proportional to $|N|^2$, thus scattering takes place to some extent for both absorbing and non-absorbing materials.

The extinction of radiation by small solid particles embedded in a continuous matrix may be analyzed by the solution of Maxwell's electromagnetic equations with

adequate boundary conditions included. The general solution of the case of a plane wave incident upon a homogeneous sphere of refractive index N_1 in a medium of refractive index N_2 was formally solved by Mie (Ref. 6). Since excellent treatments of the Mie solution are available in recent literature (Refs. 9 and 10) a complete derivation will not be included in the present report. The basic Mie equations, and a transformation of these equations to a form suitable for machine calculations by the method of Ref. 11, are presented in detail in Appendix I.

The transformed Mie equations were programmed for an IBM 7094 Computer. The machine program was used to evaluate analytically the effect of wavelength of the incident radiation, particle size (radius) and, where sufficient data were available, temperature, on the opacity parameters of small spherically symmetrical condensed systems. All particles were assumed to be embedded in a homogeneous matrix having a refractive index of unity.

In order to assess the machine program reliability, numerous preliminary calculations were performed for known cases. Results of a typical test calculation are illustrated in Fig. 1, in which the extinction efficiency factor, Q_e, is plotted against the size parameter, α. The efficiency factor, Q_e, is the ratio of the extinction cross-section in cm^2/particle to the projected geometrical area of a sphere of radius R (area $= \pi R^2$). The size parameter α is proportional to the ratio of the particle radius to the wavelength of the incident light (see Appendix I). Also indicated (circled points) are the theoretical magnitude of Q_e at various values of α as reported in Refs. 12 and 13. The agreement between the values of Q_e reported in Refs. 12 and 13 and UACRL calculations is quite satisfactory.

MATERIAL PROPERTIES

The principal properties to be considered in selecting prospective materials, either elemental or in compound form, as possible seeding agents are: nonreactivity with high-temperature hydrogen; high melting- or boiling-point temperature; and high opacity per unit mass. An analysis of the compatibility of the various high-melting-temperature, high-boiling-temperature elements and compounds with hot hydrogen is given in Ref. 14. The results of the analysis of titanium and zirconium carbides, nitrides, and oxides described in Ref. 14 indicate that compounds offer relatively little advantage with respect to useful temperature range over the elemental metals in the presence of hydrogen. As a consequence, initial selection of possible seeding agents was restricted in the present study to the chemical elements (tungsten, carbon, etc.) subject to the availability of requisite refractive index data.

Figure 2 summarizes the melting- and boiling-point temperatures for the various elements as reported in Refs. 15 and 16. The effect of temperature on the

weight percentage of typical elements in condensed states (solid and liquid) from Ref. 14 is illustrated in Fig. 3.

Because of the lack of requisite refractive index data required in the Mie analysis, a number of excellent high-temperature materials (e.g., hafnium and osmium) indicated in Fig. 2 were not studied. Conversely, refractive index data for a number of relatively low melting- or boiling-point temperature materials (e.g., aluminum and cobalt) are recorded in the current literature. These materials were included in the analysis to provide sufficient opacity parameter data in an effort to ascertain any possible trends in these variables as functions of melting- or boiling-point temperatures, density and atomic weight. A list of the materials studied and their pertinent physical properties is presented in Table I.

Where sufficient data were available, the real and imaginary parts (n and k), of the refractive index are plotted against the wavelength of the incident radiation. These data are graphically illustrated for aluminum, carbon, cobalt, iridium, molybdenum, palladium, platinum, silicon, titanium, and tungsten in Figs. 4 through 13. The circled points represent the wavelengths for which data are reported in the literature (References are noted on the figures) and for which the Mie calculations were made. For niobium, rhenium, rhodium, tantalum, and vanadium, the refractive indices are reported for only a few wavelengths. These data and the corresponding references are listed in Table II.

RESULTS OF THEORETICAL STUDY

Effect of Wavelength, Particle Size, and Temperature on the Opacity Parameters

The effect of wavelength on the extinction and absorption parameters of spherically symmetrical aluminum, carbon, cobalt, iridium, molybdenum, palladium, platinum, silicon, titanium, and tungsten particles is graphically depicted in Figs. 14 through 25. All of the data are shown for a temperature of approximately 300 K (540 R) with three exceptions: the carbon data in Fig. 15 are for a temperature of 2250 K (4050 R), and the tungsten data in Figs. 24 and 25 are for temperatures of 1100 K (1980 R) and 1600 K (2880 R), respectively. The extinction and absorption parameters for a number of particle radii (from 0.01 μ to 1.0 μ) are indicated in each figure. Values of the scattering parameters are not presented in the figures. However, this quantity is equal to the difference between the extinction and absorption parameters at any given wavelength for a specified particle size.

A typical variation with wavelength of the extinction and absorption cross-sections in cm^2/particle (the parameters expressed in cm^2/particle effectively

remove the dependence of these quantities on the particle mass -- see Appendix I) is illustrated in Fig. 26 for tungsten particles at 298 K (536 R). Similar curves may be obtained for the other species studied from the plotted data since $\sigma = b\rho V$ where b is the absorption or extinction parameter in cm^2/gm, ρ the mass density and V the particle volume.

A number of trends are evident upon examination of Figs. 14 through 26. With reference to Fig. 26, at very small particle sizes ($R \simeq 0.01\ \mu$) the scattering cross-section is negligible and absorption predominates. Extinction, in general, increases for increased particle size, as does absorption. The relative contribution of scattering to extinction, however, increases at the expense of absorption with an increase in particle size. In addition, it should be noted that the dependence of the cross-sections on wavelength is less pronounced for large particle sizes (0.5 to 1.0 μ). In Figs. 14 through 25 similar trends are observed, however, the effect of increased particle mass associated with an increase in radius tends to make larger particles less efficient absorbers and scatterers of radiation on a weight basis.

Mie calculations were also made for niobium, rhenium, rhodium, tantalum, and vanadium particles at 298 K (536 R) at selected wavelengths. Limited availability of refractive index data precluded a more thorough investigation of these materials. A summary of the refractive index data and calculated opacity parameters for particles of radius 0.01, 0.05, 0.10, 0.50, and 1.0 μ is presented in Table II.

Typical examples of the variation of the extinction and absorption parameters with particle size are illustrated in Fig. 27 for aluminum at 298 K (536 R), in Fig. 28 for carbon at 2250 K (4050 R), and in Fig. 29 for platinum at 298 K (536 R) at wavelengths between 0.4 and 2.0 μ. Similar data for tungsten at 298 K (536 R), 1100 K (1980 R), and 1600 K (2880 R) are presented in Figs. 30, 31, and 32 for the same wavelengths. As in previous figures, scattering parameters are not explicitly exhibited but may be readily inferred.

With reference to Figs. 27 through 32 in which opacity parameters are plotted against particle radius, all the curves exhibit similar behavior in that both opacity parameters increase with increasing particle size at small radii, but decrease with increasing particle size at large radii. The maximum in the curves shifts toward longer radii and simultaneously broadens as the wavelength is increased. As indicated in the previous figures (Figs. 14 through 25), absorption predominates for very small particles ($R \simeq 0.01\ \mu$) and gives way to scattering for larger particle sizes.

Refractive index data at more than one temperature were available only for tungsten. The opacity parameters of 0.1 μ-radius tungsten particles are plotted as a function of temperature in Fig. 33 for three wavelengths: 0.4, 1.0, and 2.0 μ. The effect of temperature on refractive index shown in Fig. 13 leads to a significant effect of temperature on absorption and scattering in Fig. 33 only for a wavelength of 2.0 μ.

Comparison of Opacity of Seeds Made of Different Materials

Particles which do not combine chemically with hydrogen will be effective in controlling radiant heat transfer in gaseous nuclear rocket engines at least up to the temperature at which the particles melt, and probably up to the temperature approaching that at which the particles vaporize (no information is available on the relative opacities of liquid and solid particles made of the same material). The effect of particle melting point on absorption parameter for a wavelength of approximately 0.58 microns is shown in Fig. 34 for all materials considered in the preceding sections except silicon. Although the highest absorption coefficients calculated in the program were obtained using silicon (compare data in Fig. 21 with corresponding data for other materials), no information was available which would permit calculation of the absorption parameter for silicon for wavelengths higher than 0.25 microns. However, the melting point of silicon is sufficiently low (1683 K or 2829 R) that it is not a promising material for use as a seed in gaseous nuclear rockets.

The superiority of carbon particles in terms of both absorption parameter and melting-point temperature indicated in Fig. 34 is misleading for two reasons. First, carbon sublimes at a temperature less than its melting-point temperature. Second, it is shown in Ref. 14 that graphite combines readily with hydrogen at high temperatures to form various hydrocarbon gases. Therefore, graphite is not usable as a seed material in gaseous nuclear rocket engines.

Of the remaining materials investigated, tungsten has the highest melting point (3650 K or 6570 R), although the melting point of both rhenium and tantalum are within 400 K of the melting point of tungsten. The absorption parameter for tungsten, rhenium, and tantalum are not sufficiently different to be a major factor in the choice of one of these materials over the other. However, the scarcity of rhenium makes this material an unlikely prospect for use as a seed in gaseous nuclear rockets. Use of the next highest melting point materials (molybdenum, niobium, and iridium) would result in a further reduction in melting point of approximately 500 K from that for tantalum.

Data on absorption parameter for all materials except silicon are plotted as a function of boiling point in Fig. 35. The highest boiling point is that for rhenium (5915 K or 10,650 R), but the boiling point of both tantalum and tungsten fall within 400 K of the boiling point of rhenium. Use of either niobium or molybdenum in place of tantalum or tungsten would result in a reduction in boiling point of approximately 500 K.

The absorption parameter at a wavelength of approximately 0.58 microns is plotted as a function of mass density in Fig. 36 and as a function of atomic weight in Fig. 37. Except for aluminum, most of the data indicate that absorption parameter is approximately inversely proportional to either mass density or atomic weight.

REFERENCES

1. Weinstein, H. and R. Ragsdale: The Coaxial Flow Reactor - A Gaseous Nuclear Rocket Concept. ARS Preprint 1518-60, presented at the ARS 15th Annual Meeting, Washington, D. C., December 1960.

2. Krascella, N. L.: Tables of the Composition, Opacity, and Thermodynamic Properties of Hydrogen at High Temperatures. NASA Report SP-3005, Washington, D. C., 1963.

3. Lanzo, C. D. and R. G. Ragsdale: Experimental Determination of Spectral and Total Transmissivities of Clouds of Small Particles. NASA Technical Note D-1405, September 1962.

4. Marteney, P. J.: Experimental Investigation of the Opacity of Small Particles. United Aircraft Corporation Research Laboratories Report C-910092-2, September 1964. NASA CR-211.

5. Lanzo, C. D. and R. G. Ragsdale: Heat Transfer of a Seeded Flowing Gas From an Arc Enclosed by a Quartz Tube. NASA Technical Memorandum X-52005, June 10-12, 1964.

6. Mie, G.: Annalen der Physik, Vol. 30, 1919.

7. Born, M. and E. Wolf: Principles of Optics. Pergamon Press, New York, 1959.

8. Longhurst, R. S.: Geometrical and Physical Optics. John Wiley and Sons, New York, 1957.

9. Stratton, J. A.: Electromagnetic Theory. McGraw-Hill Book Company, New York, 1941.

10. Van de Hulst, H. C.: Light Scattering by Small Particles. John Wiley and Sons, New York, 1957.

11. Aden, A. L.: Electromagnetic Scattering from Spheres with Sizes Comparable to the Wavelength. Journal of Applied Physics, Vol. 22, No. 5, May 1951.

12. Johnson, J. C. and J. R. Terrel: Transmission Cross Sections for Water Spheres Illuminated by Infrared Radiation. Journal of the Optical Society of America, Vol. 45, No. 6, June 1960.

13. Deirmendjian, D., R. Clasen and W. Viezee: Mie Scattering with Complex Index of Refraction. Journal of the Optical Society of America, Vol. 51, No. 6, June 1961.

14. Roback, R.: Thermodynamic Properties of Coolant Fluids and Particle Seeds for Gaseous Nuclear Rockets. United Aircraft Corporation Research Laboratories Report C-910092-3, September 1964. NASA CR-212.

15. Nesmeyanov, A. N.: Vapor Pressure of the Chemical Elements. Elsevier Publishing Company, New York, 1963.

16. Hodgman, C. D., et al: Handbook of Chemistry and Physics. The Chemical Rubber Publishing Company, Cleveland, Ohio, 1960-1961.

17. Gray, D. E.: American Institute of Physics Handbook. McGraw-Hill Book Company, New York, 1963.

18. Stull, V. R. and G. N. Plass: Emissivity of Dispersed Carbon Particles. Journal of the Optical Society of America, Vol. 50, No. 2, February 1960.

19. Waldron, J. P. and D. W. Juenker: Optical Properties of Clean Molybdenum. Journal of the Optical Society of America, Vol. 54, No. 2, February 1964.

20. Roberts, S.: Interpretation of the Optical Properties of Metal Surfaces. Physical Review, Vol. 100, No. 6, December 1955.

21. Philipp, H. R. and E. A. Taft: Optical Constants of Silicon in the Region 1 to 10 ev. Physical Review, Vol. 120, No. 1, October 1960.

22. Saski, T. and K. Ishiguro: Optical Constants of Silicon in the Extreme Ultraviolet Region. Physical Review, Vol. 127, No. 4, August 1962.

23. Brattain, W. H. and H. B. Briggs: Optical Constants of Germanium in the Infrared and Visible. Physical Review, Vol. 75, No. 11, June 1949.

24. Roberts, S.: Optical Properties of Nickel and Tungsten and Their Interpretation According to Drude's Formula. Physical Review, Vol. 114, No. 1, April 1959.

LIST OF SYMBOLS

a_r	Mie coefficient, dimensionless
b_r	Mie coefficient, dimensionless
b_a	Absorption parameter, $cm^2\ gm^{-1}$
b_e	Extinction parameter, $cm^2\ gm^{-1}$
b_s	Scatter parameter, $cm^2\ gm^{-1}$
$h_r^{(2)}( )$	Spherical Hankel function of the second kind
$H_{r+\frac{1}{2}}^{(2)}( )$	Circular half-order Hankel function
i	Imaginary unit = $\sqrt{-1}$
I	Intensity after incident beam traverses a length, L, of material, erg $cm^{-2}\ sec^{-1}$
I_0	Initial incident beam intensity, erg $cm^{-2}\ sec^{-1}$
$j_r( )$	Spherical Bessel function
$J_{r+\frac{1}{2}}( )$	Circular half-order Bessel function
k	Imaginary part of the refractive index, dimensionless
L	Path length, cm
n	Real part of the refractive index, dimensionless
N	Relative refractive index, dimensionless
N_1	Refractive index of the particle, dimensionless
N_2	Refractive index of the medium, dimensionless
N_i	Number density of absorbing and scattering centers, cm^{-3}
P_i	Partial pressure of species i, atm
P_t	Total pressure, atm

LIST OF SYMBOLS
(Cont.)

Q_e	Extinction efficiency factor = $\sigma_e/\pi R^2$, dimensionless
R	Particle radius, microns
T	Absolute temperature, deg K
V	Particle volume, cm^3
W_A	Atomic weight, dimensionless
W_c	Weight percentage of species c in condensed phases, dimensionless
Z	Atomic number, dimensionless
α	Size parameter = $2\pi R/\lambda$, dimensionless
λ	Wavelength of incident radiation, microns
ρ	Mass density, gm cm^{-3}
σ_a	Absorption cross-section, cm^2 $particle^{-1}$
σ_e	Extinction cross-section, cm^2 $particle^{-1}$
σ_s	Scatter cross-section, cm^2 $particle^{-1}$
ω	Wave number of incident radiation, cm^{-1}

APPENDIX I

ANALYTICAL PROCEDURE FOR ESTIMATING THE OPACITY OF SMALL SPHERICAL PARTICLES

Mie Theory

The basic Mie equations for the extinction, scattering, and absorption cross-sections of small spherical systems are (Refs. 9 and 10):

$$\sigma_e = \frac{2\pi R^2}{\alpha^2} \sum_{r=1}^{\infty} (2r+1) \ \mathrm{Re} \ (a_r + b_r) \tag{I-1}$$

$$\sigma_s = \frac{2\pi R^2}{\alpha^2} \sum_{r=1}^{\infty} (2r+1) \left(|a_r|^2 + |b_r|^2 \right) \tag{I-2}$$

$$\sigma_a = \sigma_e - \sigma_s \tag{I-3}$$

where R is the particle radius; α, a size parameter; and a_r and b_r, the Mie coefficients. The symbol " Re" denotes the real part of a complex number.

The non-dimensional size parameter α, is defined by:

$$\alpha = 2\pi R/\lambda = 2\pi R\omega \tag{I-4}$$

where λ is the wavelength of the incident radiation and ω is the reciprocal of λ or the wave number.

The Mie coefficients are analytically represented by:

$$a_r = - \frac{j_r(N\alpha) \left[\alpha j_r(\alpha)\right]' - j_r(\alpha) \left[N\alpha j_r(N\alpha)\right]'}{j_r(N\alpha) \left[\alpha h_r^{(2)}(\alpha)\right]' - h_r^{(2)}(\alpha) \left[N\alpha j_r(N\alpha)\right]'} \tag{I-5}$$

$$b_r = - \frac{j_r(\alpha) \left[N\alpha j_r(N\alpha)\right]' - N^2 j_r(N\alpha) \left[\alpha j_r(\alpha)\right]'}{h_r^{(2)}(\alpha) \left[N\alpha j_r(N\alpha)\right]' - N^2 j_r(N\alpha) \left[\alpha h_r^{(2)}(\alpha)\right]'} \tag{I-6}$$

where N is the refractive index of the particle, N_1 , relative to that of the medium, N_2 ; $j_r(\ )$, a spherical Bessel function; and $h_r^{(2)}(\ )$, a spherical Hankel function of the second kind. The primes on the brackets denote differentiation with respect to the argument of the Bessel function within the bracket:

$$\left[\alpha\, j_r(\alpha)\right]' \equiv \frac{d}{d\alpha}\left[\alpha\, j_r(\alpha)\right] \tag{I-7}$$

Note that the relative refractive index may be a complex number.

The preceding set of equations represent a summary of Mie's formal solution to the problem. Use of these equations is, in general, a formidable and tedious task. Further complications arise if the relative refractive index N is complex since extensive tables of spherical Bessel functions with complex arguments are not available. Although approximate solutions for highly specialized conditions are recorded in the literature, these are not applicable to those systems with complex refractive indices. An excellent transformation procedure, facilitating computation, is described in Ref. 11 and is presented in the following sections.

Transformation of the Mie Equations by the Logarithmic Derivative Method

According to Ref. 11, Eqs. (I-5) and (I-6) may be transformed to a new set in terms of logarithmic derivative functions. For arbitrary argument x , two new functions are defined:

$$\rho_r(x) \equiv \frac{d}{dx} \ln\left[x\, h_r^{(2)}(x)\right] \tag{I-8}$$

$$\sigma_r(x) = \frac{d}{dx} \ln\left[x\, j_r(x)\right] \tag{I-9}$$

Upon substitution of Eqs. (I-8) and (I-9) into Eqs. (I-5) and (I-6) one obtains:

$$a_r = -\frac{j_r(\alpha)}{h_r^{(2)}(\alpha)}\left[\frac{\sigma_r(\alpha) - N\sigma_r(N\alpha)}{\rho_r(\alpha) - N\sigma_r(N\alpha)}\right] \tag{I-10}$$

$$b_r = -\frac{j_r(\alpha)}{h_r^{(2)}(\alpha)} \left[\frac{\sigma_r(N\alpha) - N\sigma_r(\alpha)}{\sigma_r(N\alpha) \quad N\rho_r(\alpha)} \right] \tag{I-11}$$

Since α is always a real quantity the ratio $j_r(\alpha)/h_r^{(2)}(\alpha)$ may be evaluated with the aid of standard spherical Bessel functions tables or with the aid of standard recursion formulas. The recursion formulas are mathematically defined as follows:

The spherical Bessel and Hankel functions may be described in terms of the half-order circular Bessel and Hankel functions. These are:

$$j_r(\alpha) = \sqrt{\pi/2\alpha} \quad J_{r+\frac{1}{2}}(\alpha) \tag{I-12}$$

$$h_r^{(2)}(\alpha) = \sqrt{\pi/2\alpha} \quad H_{r+\frac{1}{2}}^{(2)}(\alpha) \tag{I-13}$$

where $J_{r+\frac{1}{2}}(\alpha)$ and $H_{r+\frac{1}{2}}^{(2)}(\alpha)$ are the half-order functions. $J_{r+\frac{1}{2}}(\alpha)$ and $H_{r+\frac{1}{2}}^{(2)}(\alpha)$ are in turn defined by the following recursion equations:

$$J_{r+\frac{1}{2}}(\alpha) = \frac{2r-1}{\alpha} J_{r-\frac{1}{2}}(\alpha) - J_{r-\frac{3}{2}}(\alpha) \tag{I-14}$$

$$H_{r+\frac{1}{2}}^{(2)}(\alpha) = \frac{2r-1}{\alpha} H_{r-\frac{1}{2}}^{(2)}(\alpha) - H_{r-\frac{3}{2}}^{(2)}(\alpha) \tag{I-15}$$

where

$$J_{\frac{1}{2}}(\alpha) = \sqrt{2/\pi\alpha} \quad \text{SIN } \alpha \tag{I-16}$$

$$J_{-\frac{1}{2}}(\alpha) = \sqrt{2/\pi\alpha} \quad \text{COS } \alpha \tag{I-17}$$

$$H_{\frac{1}{2}}^{(2)}(\alpha) = \sqrt{2/\pi\alpha} \quad \frac{e^{i\alpha}}{i} \tag{I-18}$$

$$H^{(2)}_{-\frac{1}{2}}(\alpha) = \sqrt{2/\pi\alpha}\; e^{-i\alpha} \tag{I-19}$$

Substitution of Eqs. (I-14) and (I-15) into Eqs. (I-12) and (I-13) respectively gives the required recursion formulas for $j_r(\alpha)$ and $h_r^{(2)}(\alpha)$:

$$j_r(\alpha) = \sqrt{\pi/2\alpha}\left[\frac{2r-1}{\alpha} J_{r-\frac{1}{2}}(\alpha) - J_{r-\frac{3}{2}}(\alpha)\right] \tag{I-20}$$

$$h_r^{(2)}(\alpha) = \sqrt{\pi/2\alpha}\left[\frac{2r-1}{\alpha} H^{(2)}_{r-\frac{1}{2}}(\alpha) - H^{(2)}_{r-\frac{3}{2}}(\alpha)\right] \tag{I-21}$$

The quantities $\rho_r(\alpha)$, $\sigma_r(\alpha)$, and $\sigma_r(N\alpha)$ are readily evaluated by means of the following alternate forms of Eqs. (I-8) and (I-9):

$$\rho_r(\alpha) = \frac{h^{(2)}_{r-1}(\alpha)}{h_r{}^2(\alpha)} - \frac{r}{\alpha} \tag{I-22}$$

$$\sigma_r(\alpha) = \frac{j_{r-1}(\alpha)}{j_r(\alpha)} - \frac{r}{\alpha} \tag{I-23}$$

$$\sigma_r(N\alpha) = \frac{(N\alpha)^2 + r(N\alpha)\,\sigma_{r-1}(N\alpha) - r^2}{r(N\alpha) - (N\alpha)^2\,\sigma_{r-1}(N\alpha)} \tag{I-24}$$

where $$\sigma_0(N\alpha) = \cot(N\alpha) \tag{I-25}$$

If the relative refractive index is a complex quantity, then Eq. (I-25) becomes

$$\sigma_0(N\alpha) = \cot(n-ik)\alpha \tag{I-26}$$

where $N \equiv n - ik$ (I-27)

The preceding equations were used to develop a machine program which would allow calculation of σ_a, σ_e, and σ_s in cm^2 $particle^{-1}$ as a function of material, wavelength or wave number, index of refraction and particle radius. The mass density of the material was also inputted as part of the program to allow determination of the opacity parameters b_a, b_e, and b_s in cm^2 gm^{-1}. The opacity parameters are given by:

$$b_a = \sigma_a / \rho V \quad \text{(I-28)}$$

$$b_e = \sigma_e / \rho V \quad \text{(I-29)}$$

$$b_s = \sigma_s / \rho V \quad \text{(I-30)}$$

where ρ is the mass density and V is the volume of the spherical particle of radius R.

TABLE I

PHYSICAL PROPERTIES OF ELEMENTS CONSIDERED IN THE MIE CALCULATIONS

Data from Refs. 15 and 16

(S - Sublimes)

Seed Material	Symbol	Melting-Point Temperature		Boiling-Point Temperature		Mass Density		Atomic Weight	n, k, b_e, & b_a Data in Figures or Tables	Wavelength Range Studied μ
		Deg K	Deg R	Deg K	Deg R	gm/cm^3	lb/ft^3			
Aluminum	Al	932	1668	2621	4718	2.70	168	27.0	4, 14, 27	0.222 to 6.0
Carbon	C	4200-S	7560-S	-	-	2.00	125	12.0	5, 15, 28	0.40 to 4.0
Cobalt	Co	1768	3182	2528	4550	8.90	555	58.9	6, 16	0.231 to 2.25
Iridium	Ir	2727	4909	4450	8010	22.40	1398	192.2	7, 17	0.579 to 4.60
Molybdenum	Mo	2890	5202	5100	9180	10.20	636	96.0	8, 18	0.248 to 0.577
Niobium	Nb	2770	4986	5115	9207	8.55	534	92.9	II	0.579
Palladium	Pd	1823	3281	3385	6093	11.97	747	106.4	9, 19	0.302 to 0.578
Platinum	Pt	2043	3677	3980	7164	21.45	1338	195.1	10, 20, 29	0.25 to 4.0
Rhenium	Re	3453	6215	5915	10647	20.53	1281	186.2	II	0.436, 0.589
Rhodium	Rh	2239	4030	3940	7092	12.4	774	102.9	II	0.546, 0.579, 0.660
Silicon	Si	1683	3029	2890	5202	2.40	151	28.1	11, 21	0.0855 to 0.248
Tantalum	Ta	3270	5886	5565	10017	16.60	1036	181.0	II	0.578
Titanium	Ti	1963	3533	3444	6199	4.50	281	47.9	12, 22	0.436 to 0.650
Tungsten	W	3650	6570	5645	10161	19.30	1204	183.9	13, 23, 24, 25, 30, 31, 32, 33	0.4 to 4.0
Vanadium	V	2190	3942	3273	5891	5.96	372	51.0	II	0.579

TABLE II

SUBSIDIARY OPACITY PARAMETER RESULTS

Data from Ref. 17

T = 298 K (536 R)

Element	Symbol	Wavelength λ μ	Refractive Index n	Refractive Index k	Radius R μ	Extinction Parameter b_e cm^2/gm	Absorption Parameter b_a cm^2/gm
Niobium	Nb	0.579	1.80	2.11	0.01	1.53×10^4	1.52×10^4
					0.05	2.69×10^4	2.17×10^4
					0.10	2.98×10^4	1.45×10^4
					0.50	4.83×10^3	1.78×10^3
					1.00	2.21×10^3	7.51×10^2
Rhenium	Re	0.436	2.62	2.97	0.01	4.45×10^3	4.41×10^3
					0.05	1.64×10^4	9.30×10^3
					0.10	1.11×10^4	4.18×10^3
					0.50	1.87×10^3	5.69×10^2
					1.00	8.76×10^2	2.50×10^2
		0.589	3.18	3.55	0.01	2.25×10^3	2.24×10^3
					0.05	7.25×10^3	5.12×10^3
					0.10	1.20×10^4	4.31×10^3
					0.50	1.90×10^3	5.35×10^2
					1.00	8.86×10^2	2.34×10^2
Rhodium	Rh	0.546	1.62	4.63	0.01	2.73×10^3	2.70×10^3
					0.05	1.18×10^4	5.67×10^3
					0.10	2.02×10^4	3.95×10^3
					0.50	3.20×10^3	5.25×10^2
					1.00	1.50×10^3	2.35×10^2
		0.579	1.54	4.67	0.01	2.43×10^3	2.40×10^3
					0.05	9.64×10^3	4.90×10^3
					0.10	2.07×10^4	4.00×10^3
					0.50	3.22×10^3	5.10×10^2
					1.00	1.51×10^3	2.28×10^2
		0.660	1.81	5.32	0.01	1.64×10^3	1.63×10^3
					0.05	5.94×10^3	3.43×10^3
					0.10	1.88×10^4	3.83×10^3
					0.50	3.18×10^3	4.67×10^2
					1.00	1.49×10^3	2.08×10^2
Tantalum	Ta	0.578	2.05	2.32	0.01	6.34×10^3	6.33×10^3
					0.05	1.25×10^4	9.79×10^3
					0.10	1.54×10^4	7.04×10^3
					0.50	2.46×10^3	8.72×10^2
					1.00	1.13×10^3	3.71×10^2

TABLE II
(Cont.)

Element	Symbol	Wavelength λ μ	Refractive Index n	Refractive Index k	Radius R μ	Extinction Parameter b_e cm^2/gm	Absorption Parameter b_a cm^2/gm
Vanadium	V	0.579	3.03	3.51	0.01	8.32×10^3	8.27×10^3
					0.05	2.63×10^4	1.83×10^4
					0.10	4.14×10^4	1.48×10^4
					0.50	6.56×10^3	1.85×10^3
					1.00	3.06×10^3	8.10×10^2

EFFECT OF RELATIVE SIZE PARAMETER ON THE EXTINCTION EFFICIENCY FACTOR AS REPORTED IN THE LITERATURE AND COMPARED WITH UACRL MACHINE CALCULATIONS

N = 1.29 − 0.0645i

CURVE DETERMINED BY UACRL MACHINE PROGRAM

NOTE { FIRST LINE — DATA FROM REF. 12
SECOND LINE — DATA FROM REF. 13
THIRD LINE — DATA FROM UACRL MIE THEORY PROGRAM

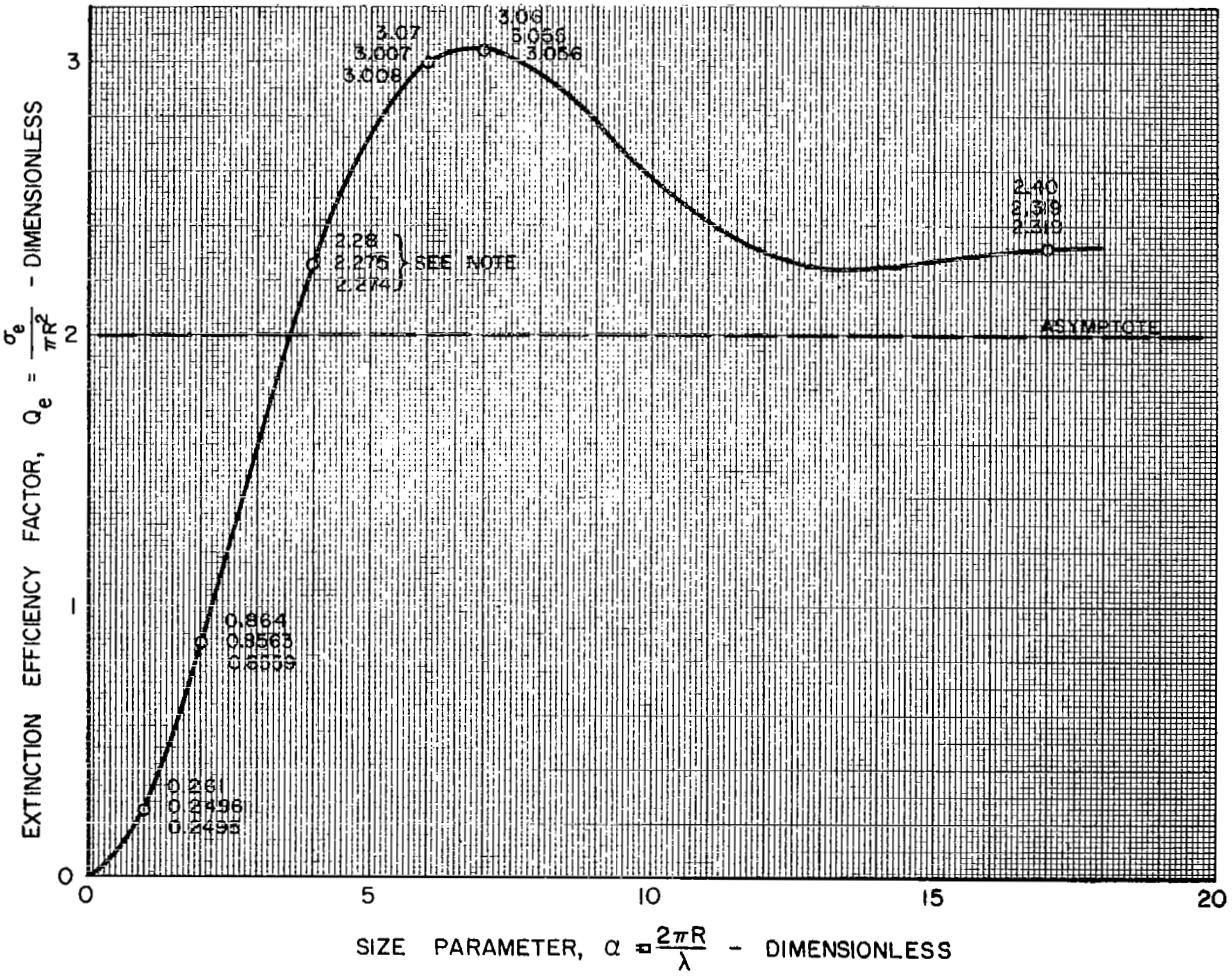

Figure 1

VARIATION OF MELTING - AND BOILING - POINT TEMPERATURE OF THE ELEMENTS WITH ATOMIC NUMBER

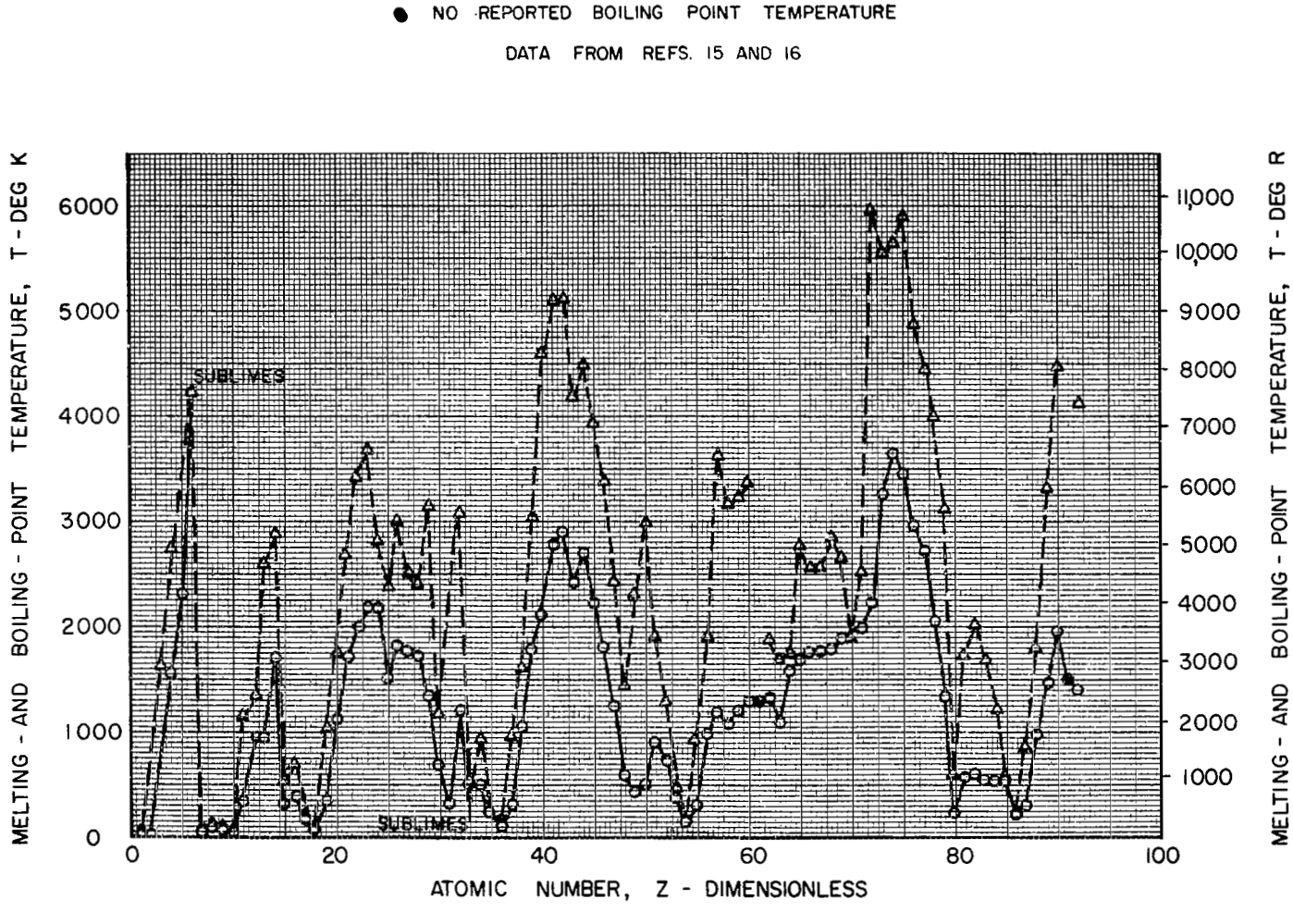

Figure 2

EFFECT OF TEMPERATURE ON THE WEIGHT PERCENTAGE OF POSSIBLE SEED MATERIALS IN CONDENSED PHASES

(2 % SEED BY WEIGHT IN HYDROGEN AT 1000 ATM)

DATA FROM REF. 14

NUMBERS IN PARENTHESIS INDICATE MELTING - POINT TEMPERATURES IN DEG K

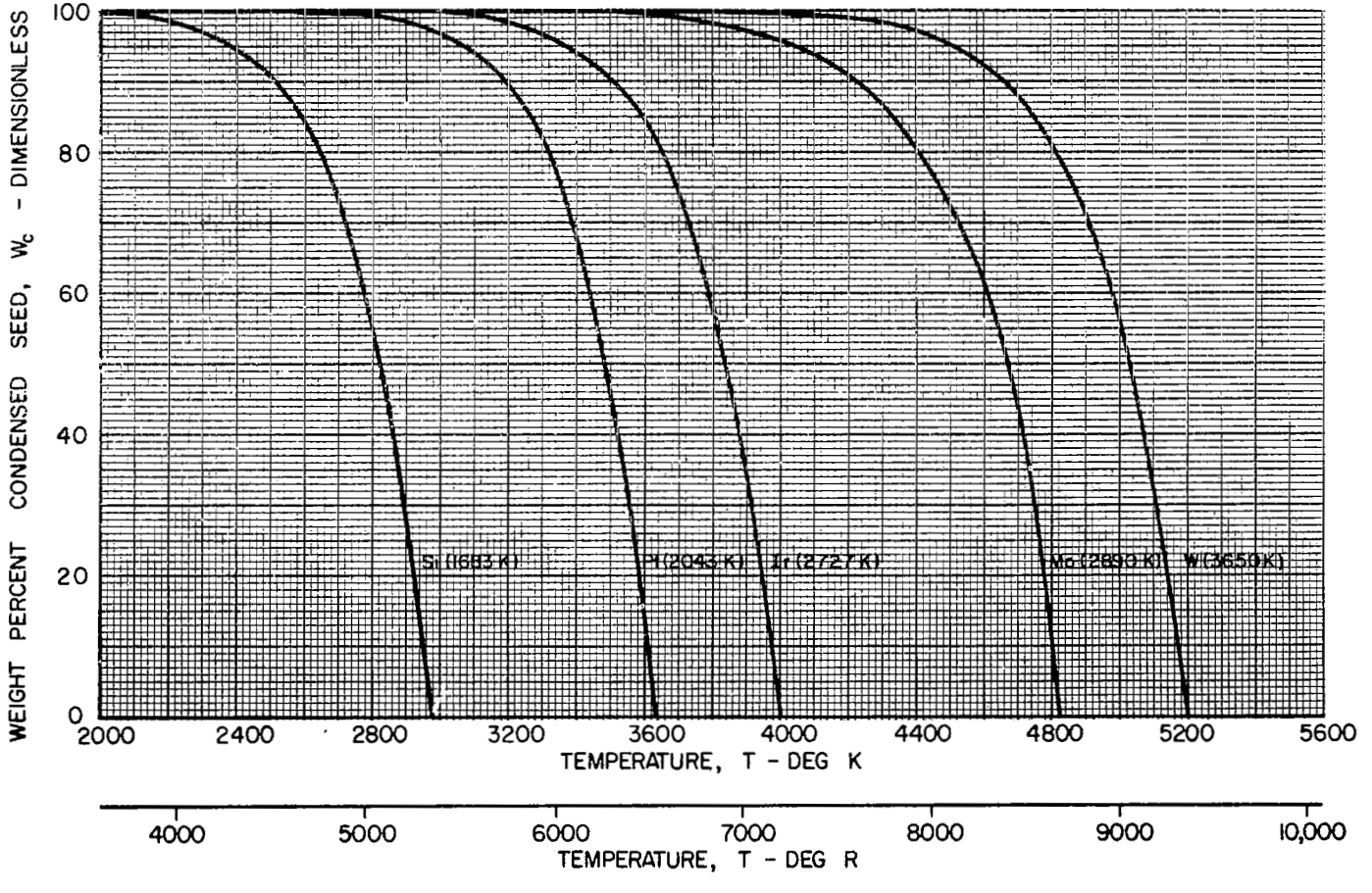

Figure 3

EFFECT OF WAVELENGTH ON THE REAL AND IMAGINARY PARTS OF THE REFRACTIVE INDEX OF ALUMINUM

T = 298 K (536 R)

N = n - ik

o - INDICATES POINTS WHICH WERE OBTAINED FROM REF. 17 AND WHICH WERE USED IN THE MIE THEORY CALCULATIONS

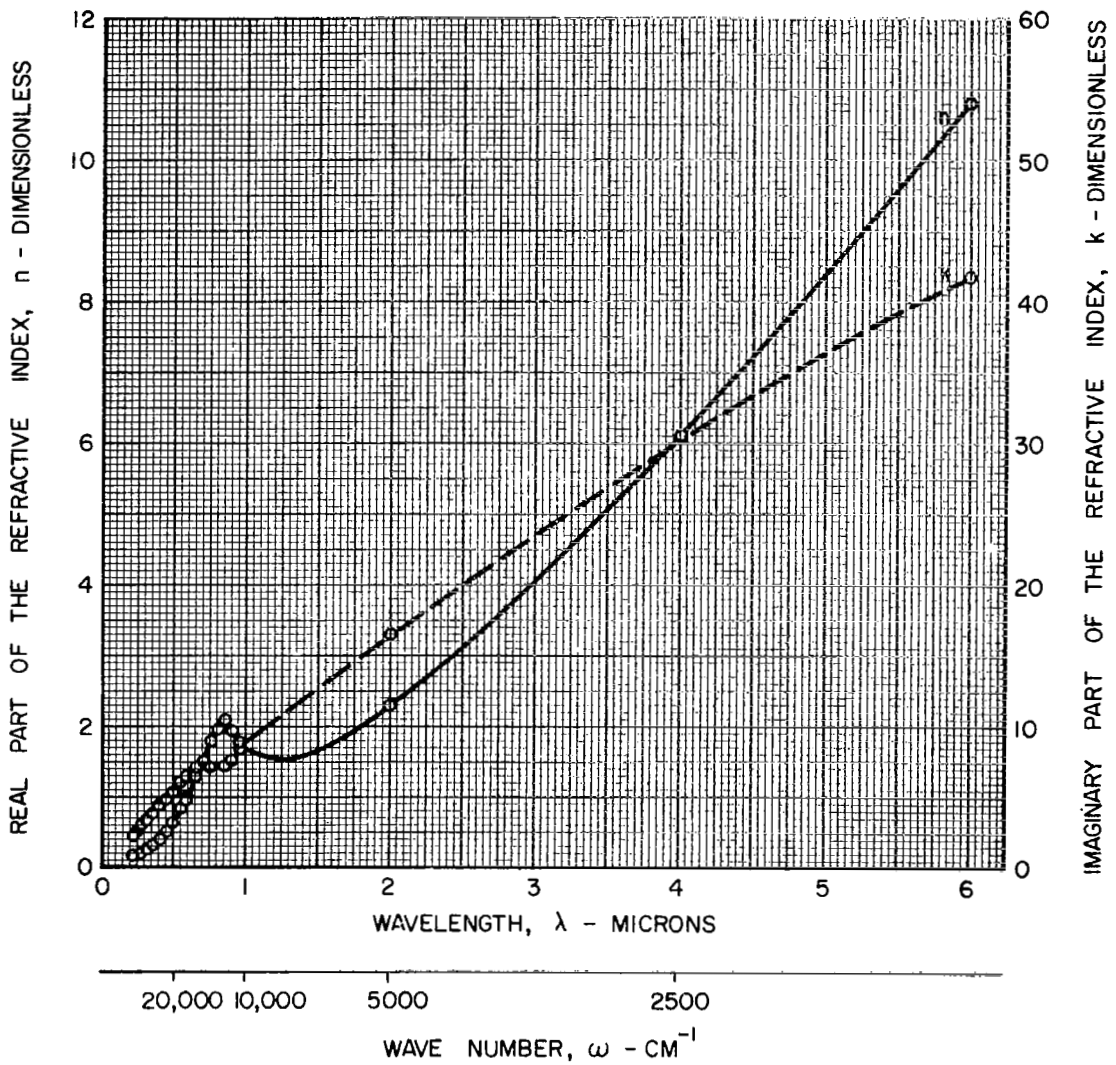

Figure 4

EFFECT OF WAVELENGTH ON THE REAL AND IMAGINARY PARTS OF THE REFRACTIVE INDEX OF CARBON

T = 2250 K (4050 R) N = n - ik

o - INDICATES POINTS WHICH WERE OBTAINED FROM REF. 18 AND WHICH WERE USED IN THE MIE THEORY CALCULATIONS

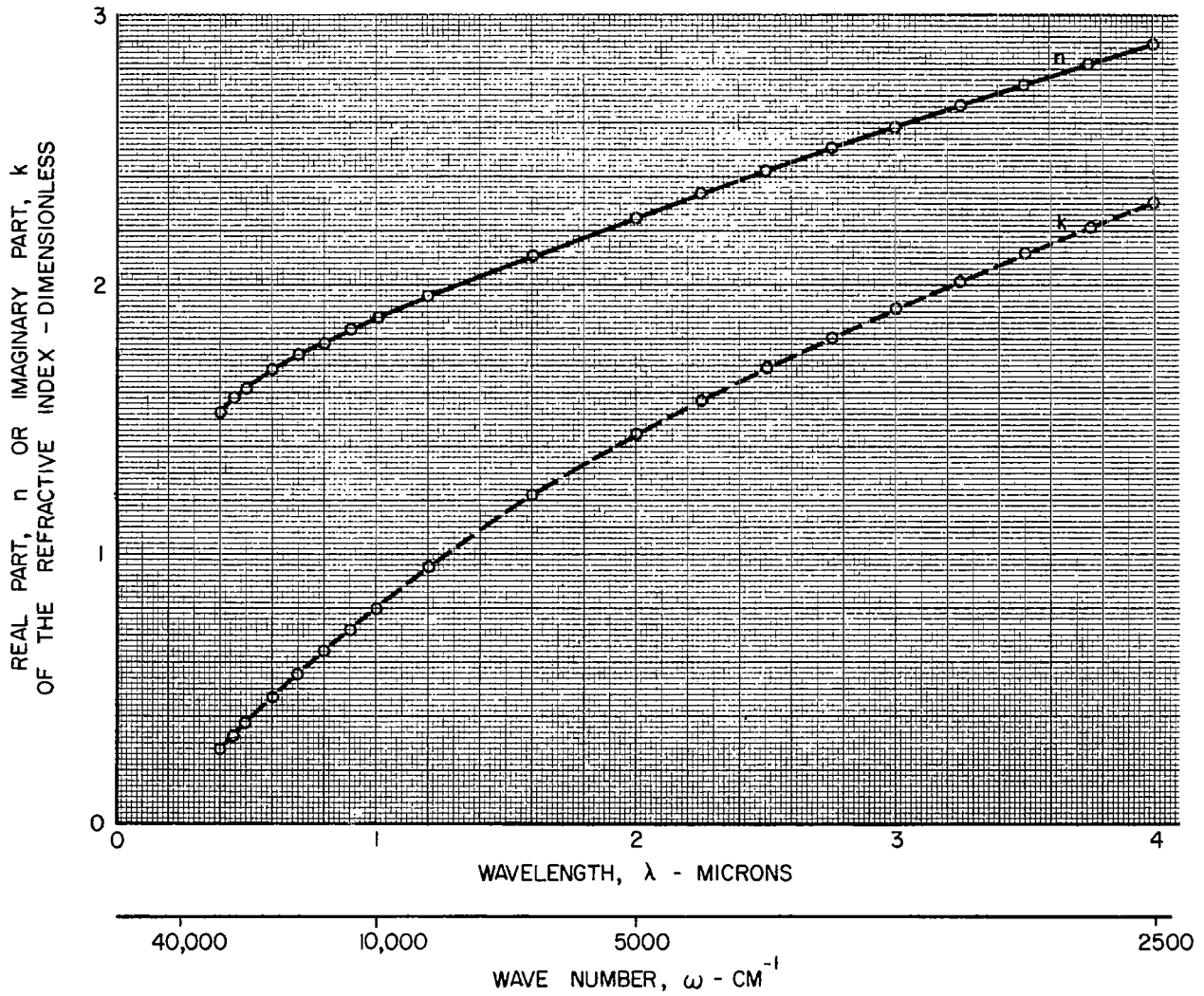

Figure 5

EFFECT OF WAVELENGTH ON THE REAL AND IMAGINARY PARTS OF THE REFRACTIVE INDEX OF COBALT

T= 298 K (536 R)

N= n-ik

o - INDICATES POINTS WHICH WERE OBTAINED FROM REF. 17 AND WHICH WERE USED IN THE MIE THEORY CALCULATIONS

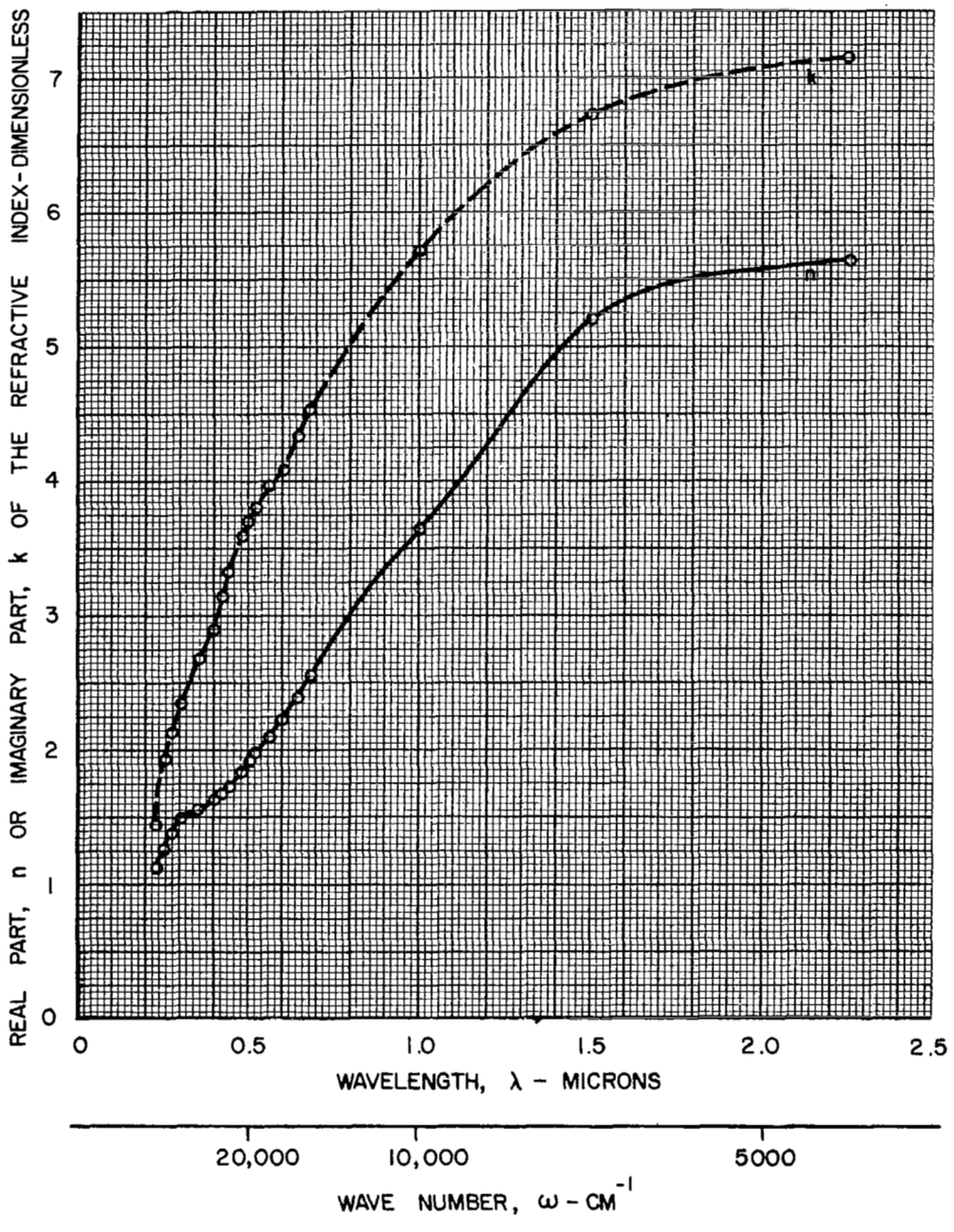

Figure 6

EFFECT OF WAVELENGTH ON THE REAL AND IMAGINARY PARTS OF THE REFRACTIVE INDEX OF IRIDIUM

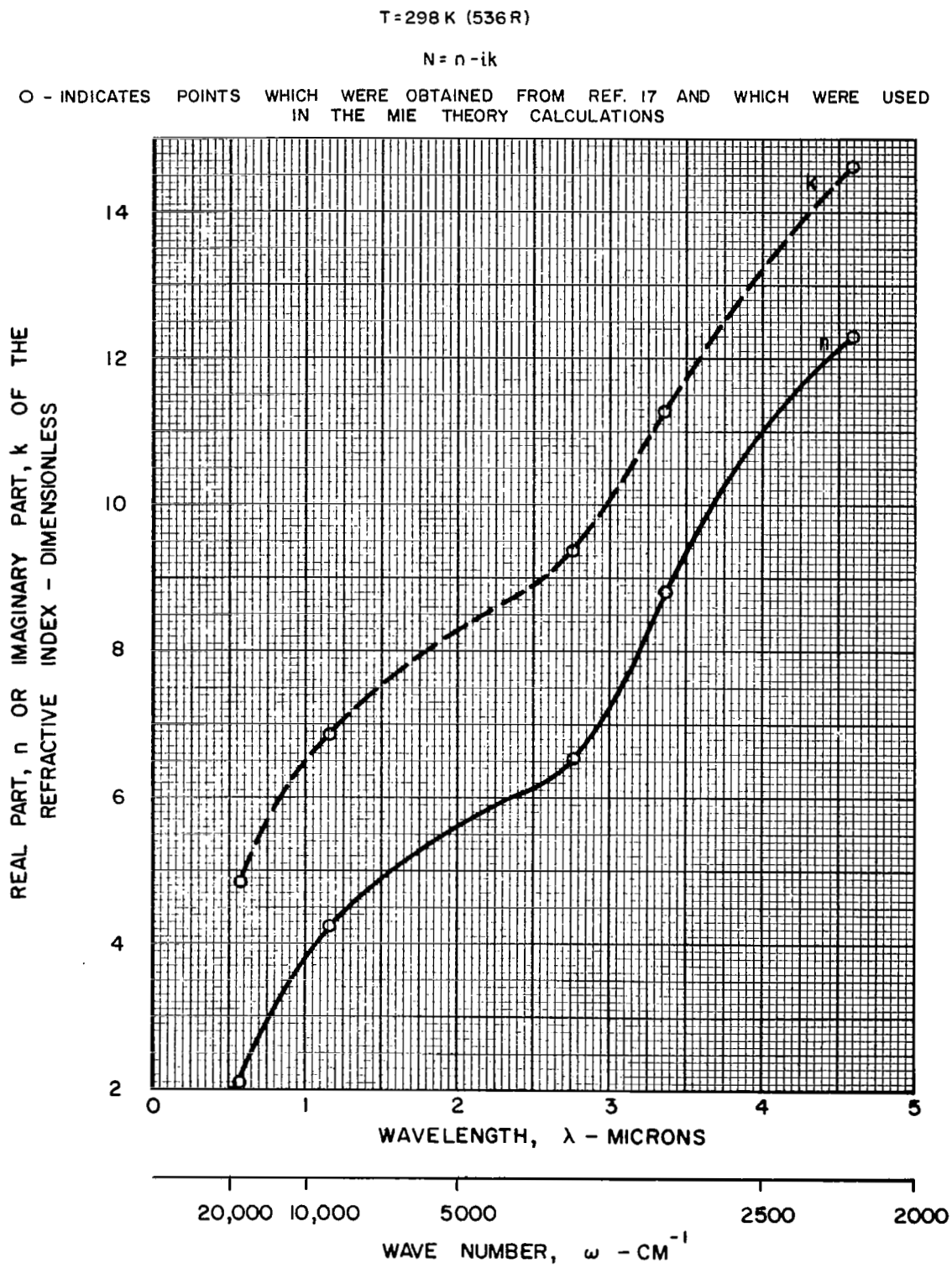

Figure 7

EFFECT OF WAVELENGTH ON THE REAL AND IMAGINARY PARTS OF THE REFRACTIVE INDEX OF MOLYBDENUM

T = 298K (536R)

N = n - ik

O - INDICATES POINTS WHICH WERE OBTAINED FROM REF. 19 AND WHICH WERE USED IN THE MIE THEORY CALCULATION

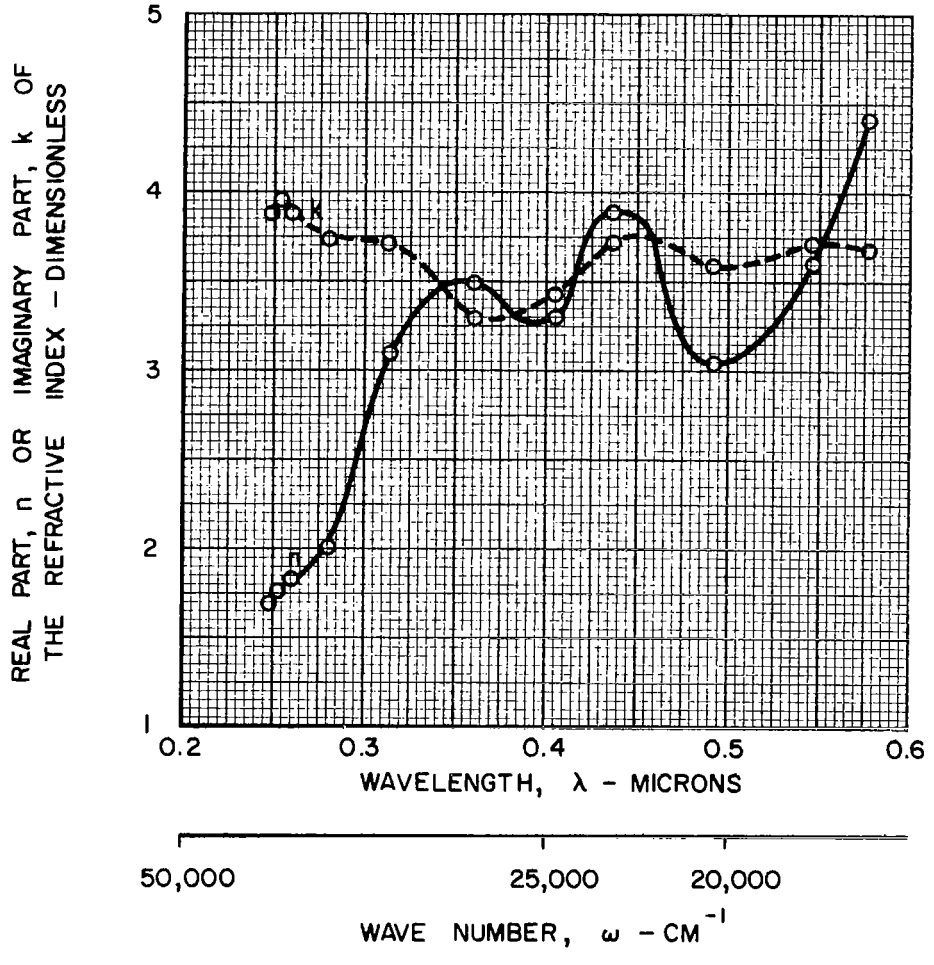

Figure 8

EFFECT OF WAVELENGTH ON THE REAL AND IMAGINARY PARTS OF THE REFRACTIVE INDEX OF PALLADIUM

T = 298 K (536 R)

N = n - ik

o - INDICATES POINTS WHICH WERE OBTAINED FROM REF. 17 AND WHICH WERE USED IN THE MIE THEORY CALCULATIONS

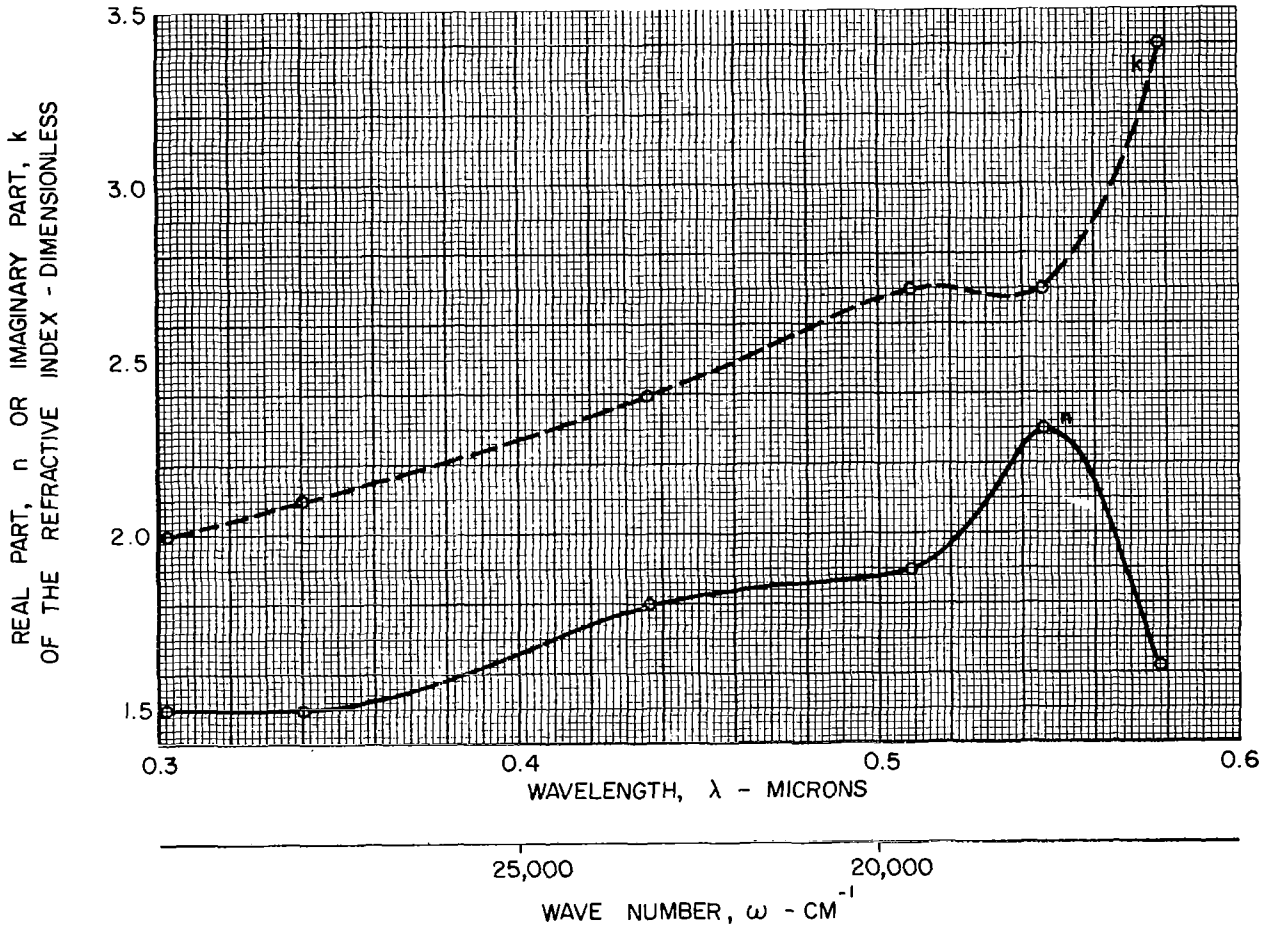

Figure 9

EFFECT OF WAVELENGTH ON THE REAL AND IMAGINARY PARTS OF THE REFRACTIVE INDEX OF PLATINUM

T = 298 K (536 R)

N = n - ik

o - INDICATES POINTS WHICH WERE OBTAINED FROM REF. 20 AND WHICH WERE USED IN THE MIE THEORY CALCULATIONS

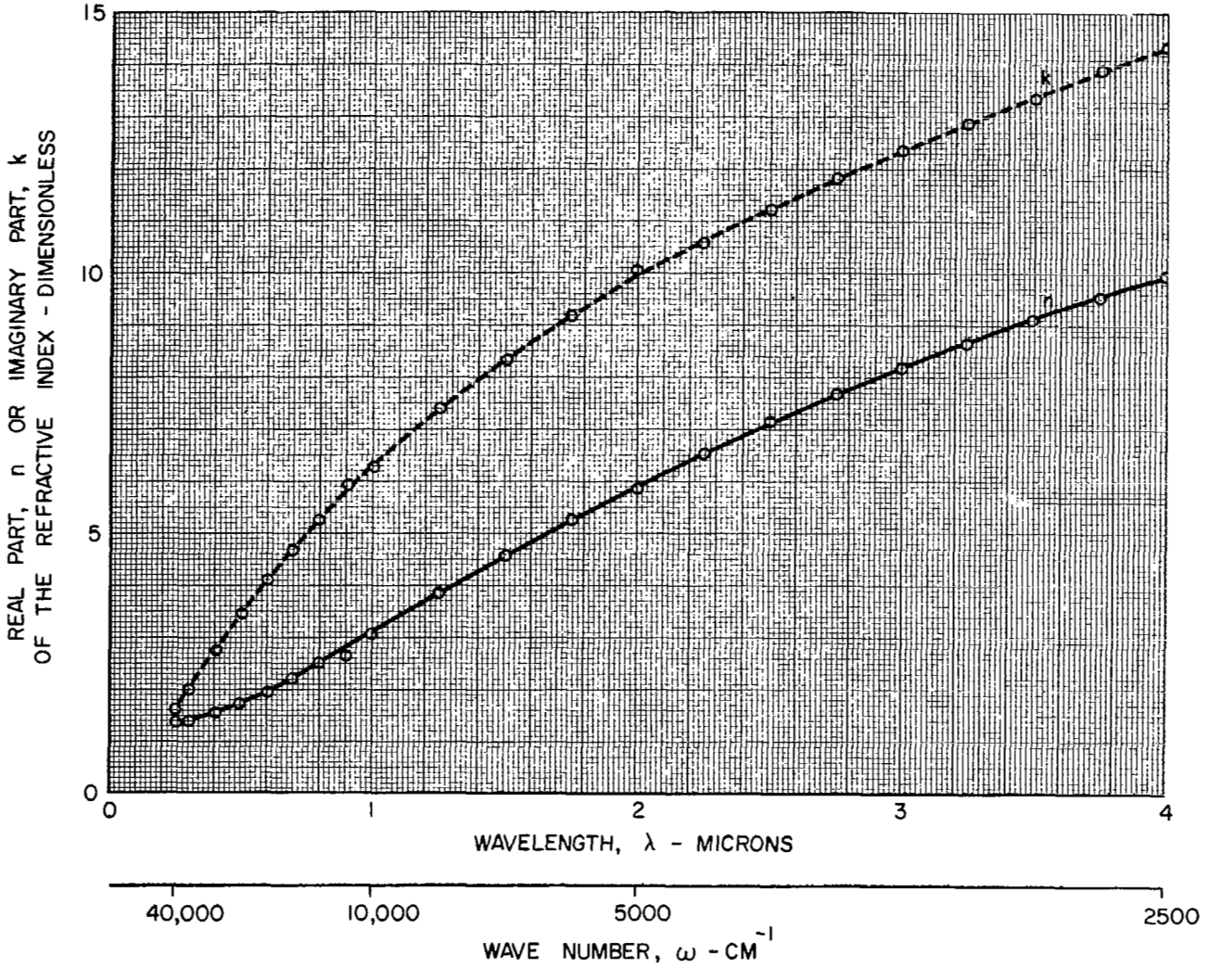

Figure 10

EFFECT OF WAVELENGTH ON THE REAL AND IMAGINARY PARTS OF THE REFRACTIVE INDEX OF SILICON

T = 300 K (540 R)

N = n - ik

o - INDICATES POINTS WHICH WERE OBTAINED FROM REFS. 21, 22, 23 AND WHICH WERE USED IN THE MIE THEORY CALCULATIONS

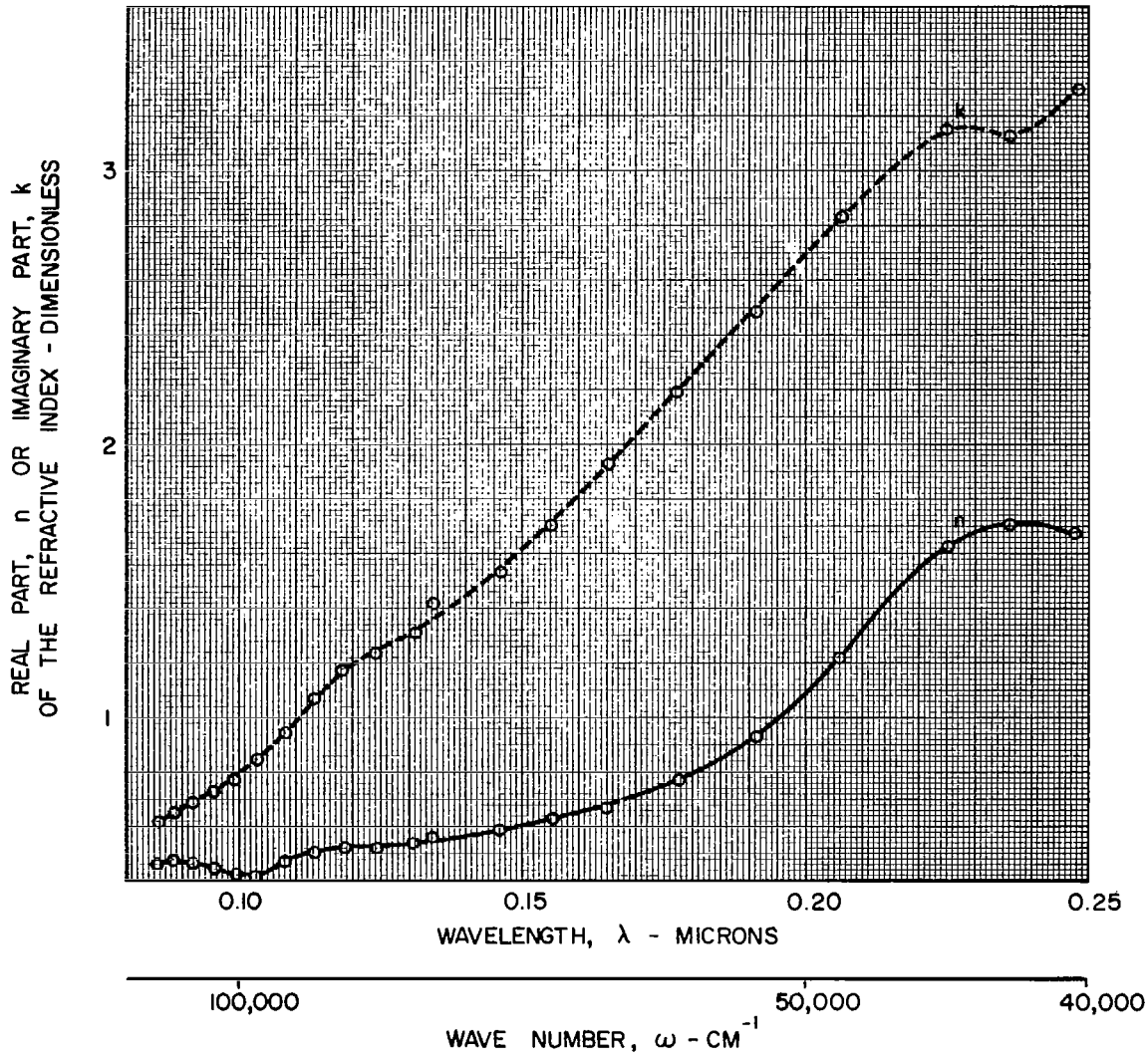

Figure 11

EFFECT OF WAVELENGTH ON THE REAL AND IMAGINARY PARTS OF THE REFRACTIVE INDEX OF TITANIUM

T = 298 K (536 R)

N = n - ik

o - INDICATES POINTS WHICH WERE OBTAINED FROM REF. 17 AND WHICH WERE USED IN THE MIE THEORY CALCULATIONS

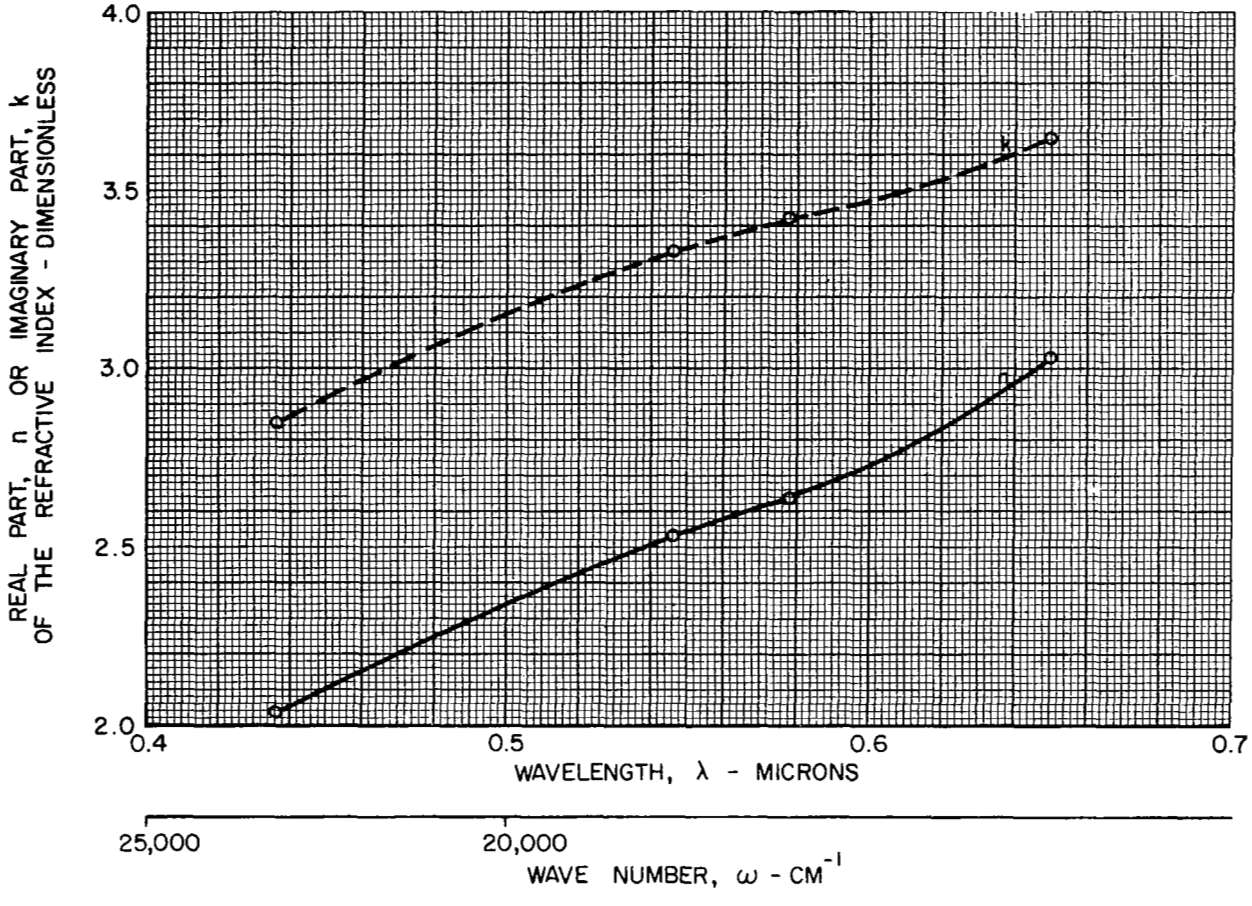

Figure 12

EFFECT OF WAVELENGTH ON THE REAL AND IMAGINARY PARTS OF THE REFRACTIVE INDEX OF TUNGSTEN

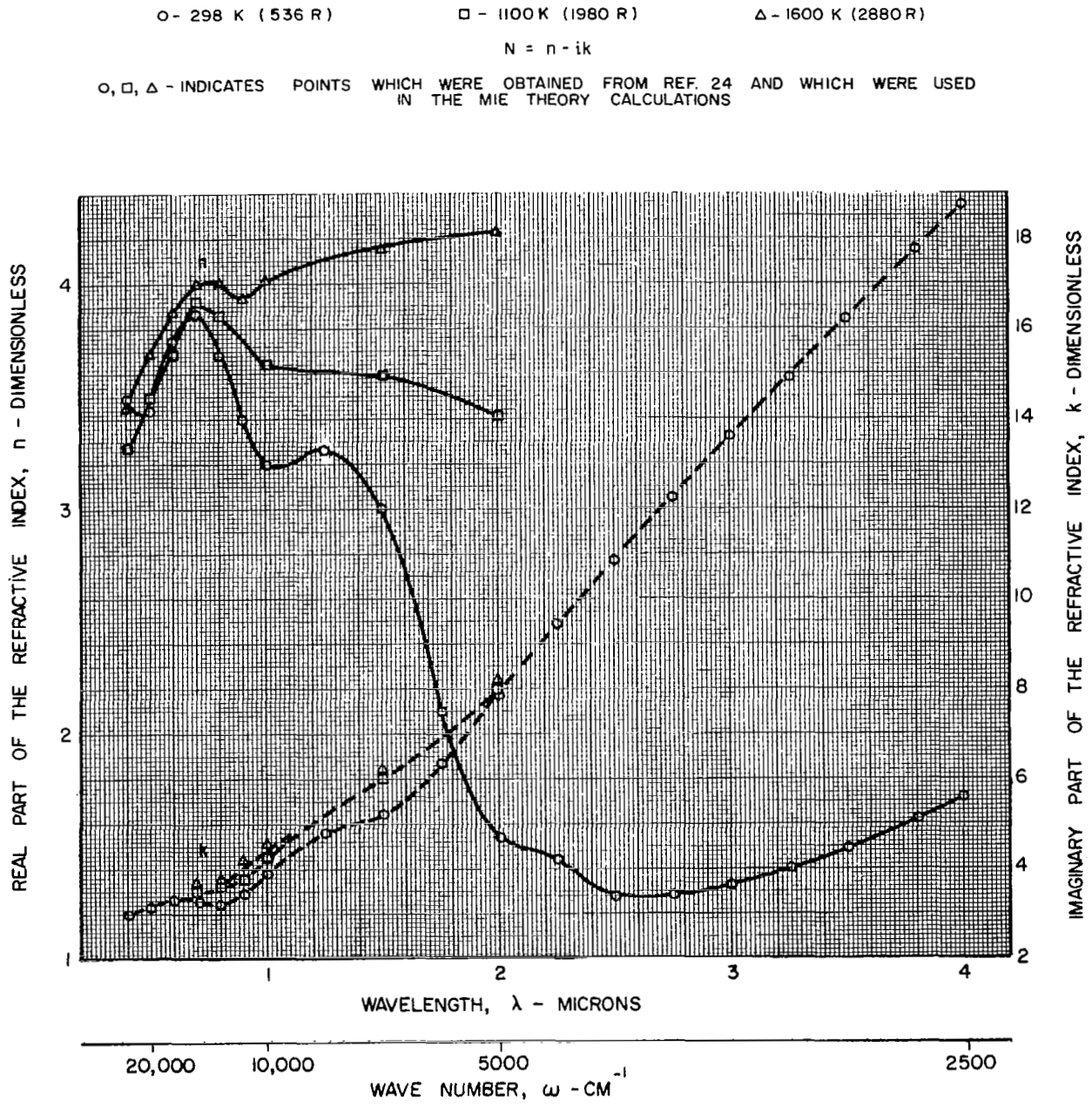

Figure 13

EFFECT OF WAVELENGTH ON THE EXTINCTION AND ABSORPTION PARAMETERS OF SPHERICAL ALUMINUM PARTICLES

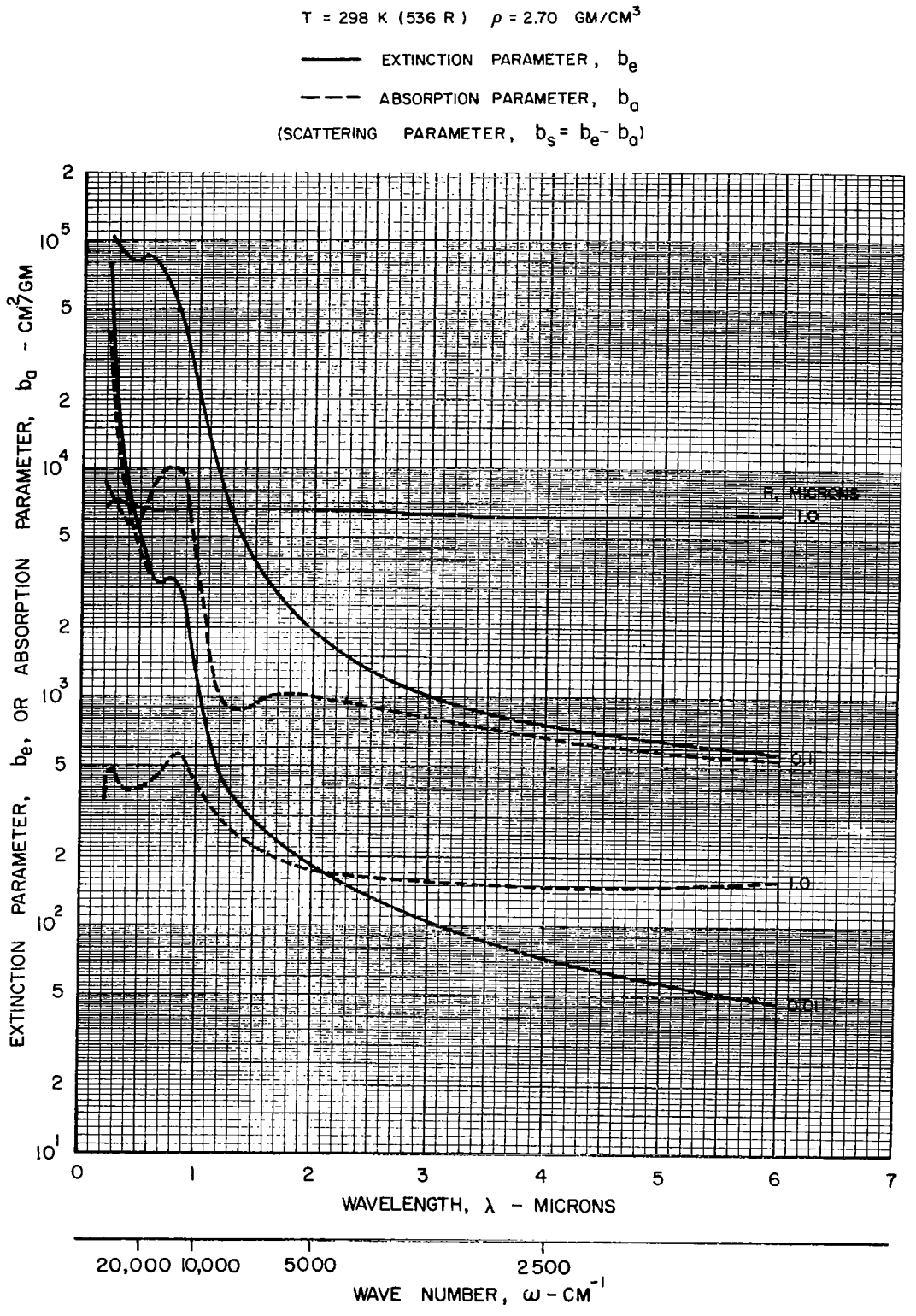

Figure 14

EFFECT OF WAVELENGTH ON THE EXTINCTION AND ABSORPTION PARAMETERS OF SPHERICAL CARBON PARTICLES

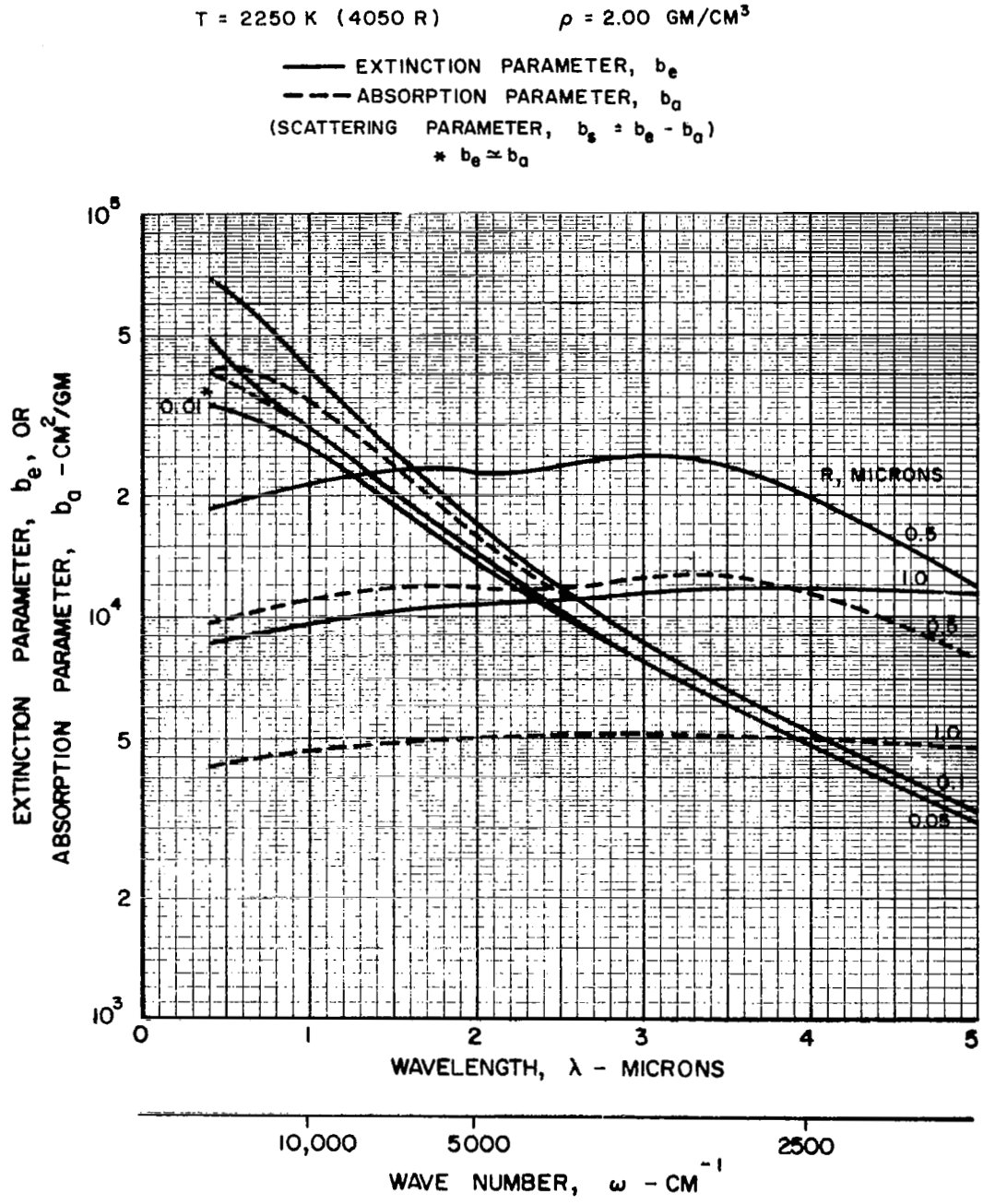

Figure 15

EFFECT OF WAVELENGTH ON THE EXTINCTION AND ABSORPTION PARAMETERS OF SPHERICAL COBALT PARTICLES

T = 298 K (536 R) ρ = 8.90 GM/CM^3

—— EXTINCTION PARAMETER, b_e

– – – ABSORPTION PARAMETER, b_a

(SCATTERING PARAMETER, $b_s = b_e - b_a$)

* $b_e \simeq b_a$

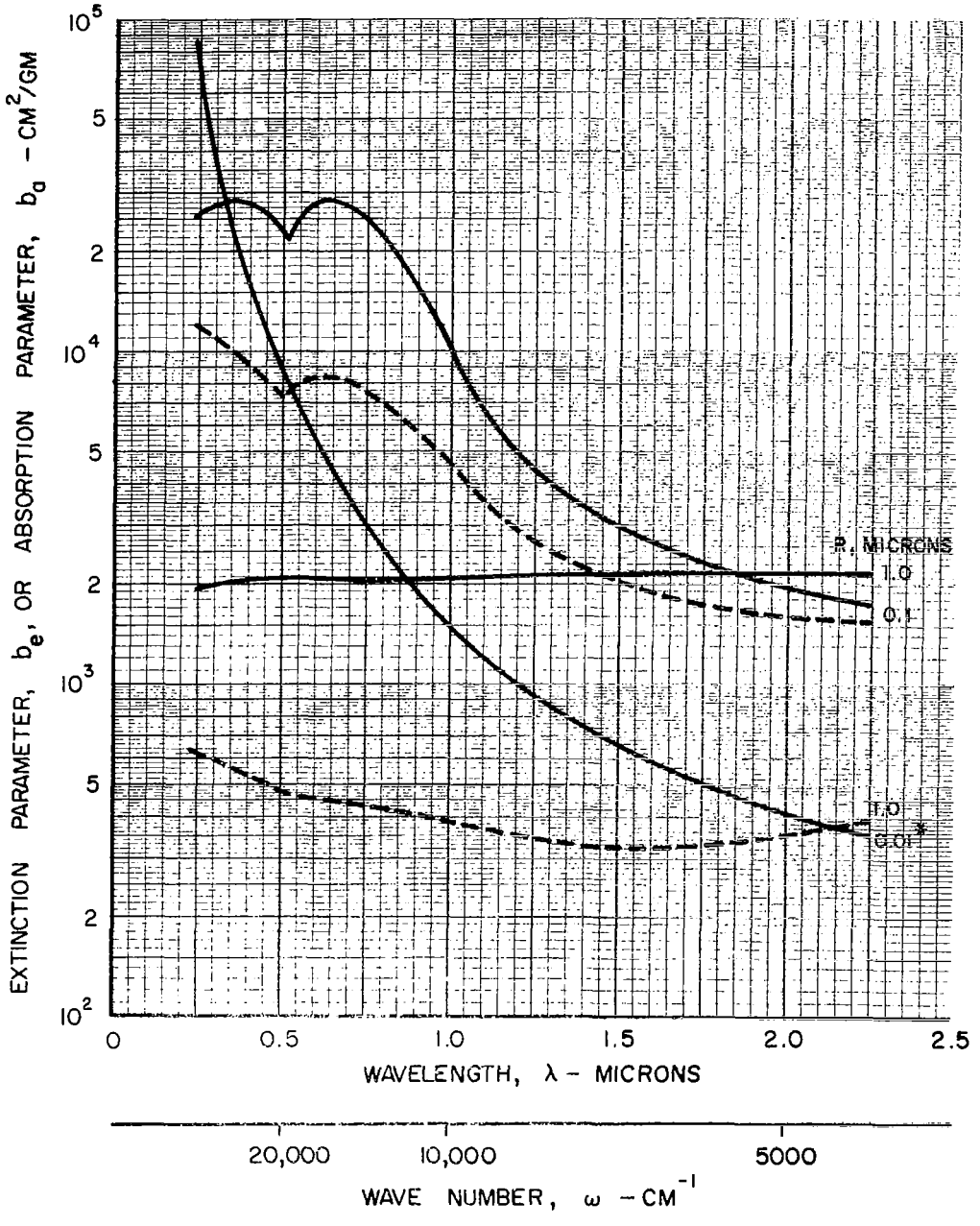

Figure 16

EFFECT OF WAVELENGTH ON THE EXTINCTION AND ABSORPTION PARAMETERS OF SPHERICAL IRIDIUM PARTICLES

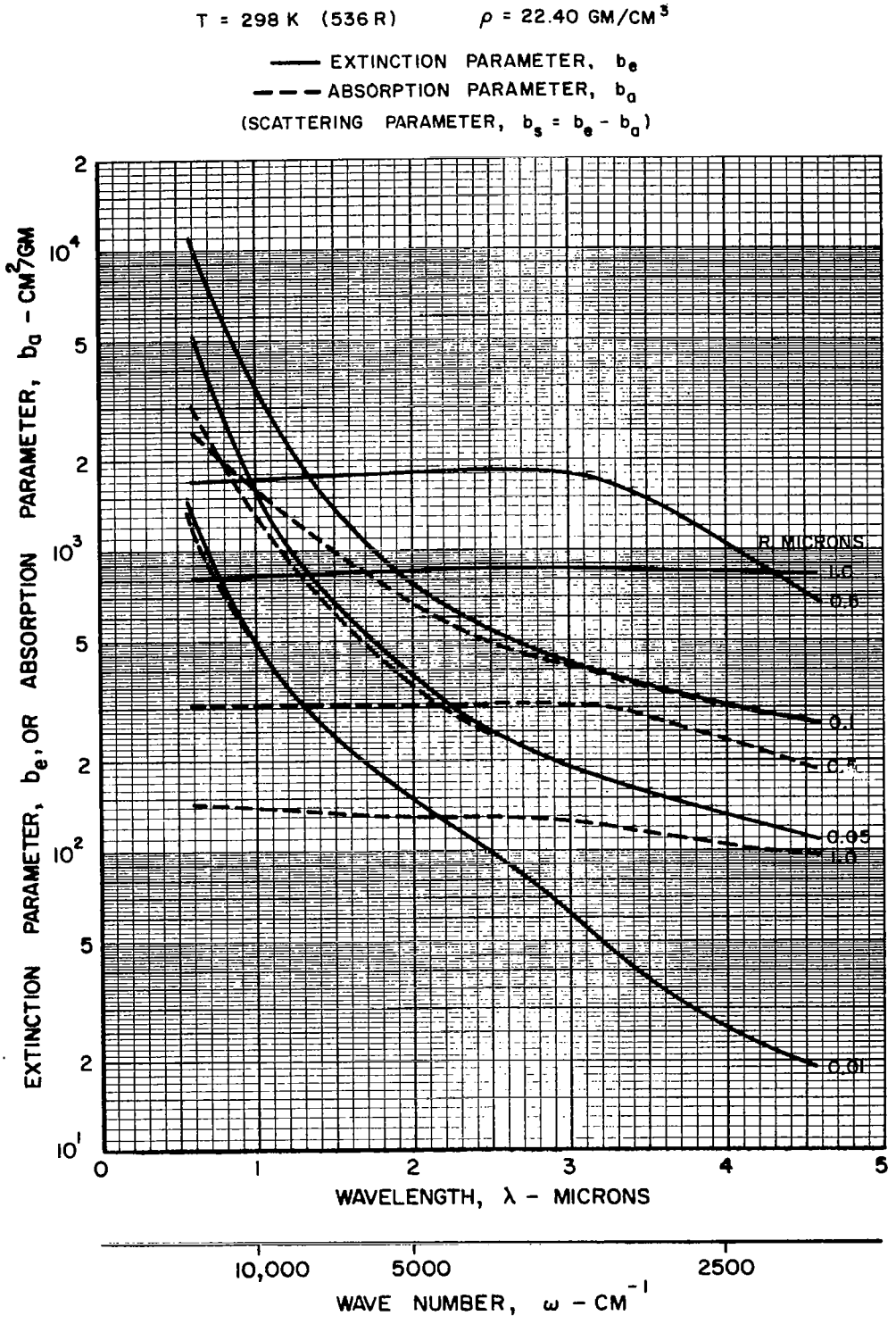

Figure 17

EFFECT OF WAVELENGTH ON THE EXTINCTION AND ABSORPTION PARAMETERS OF SPHERICAL MOLYBDENUM PARTICLES

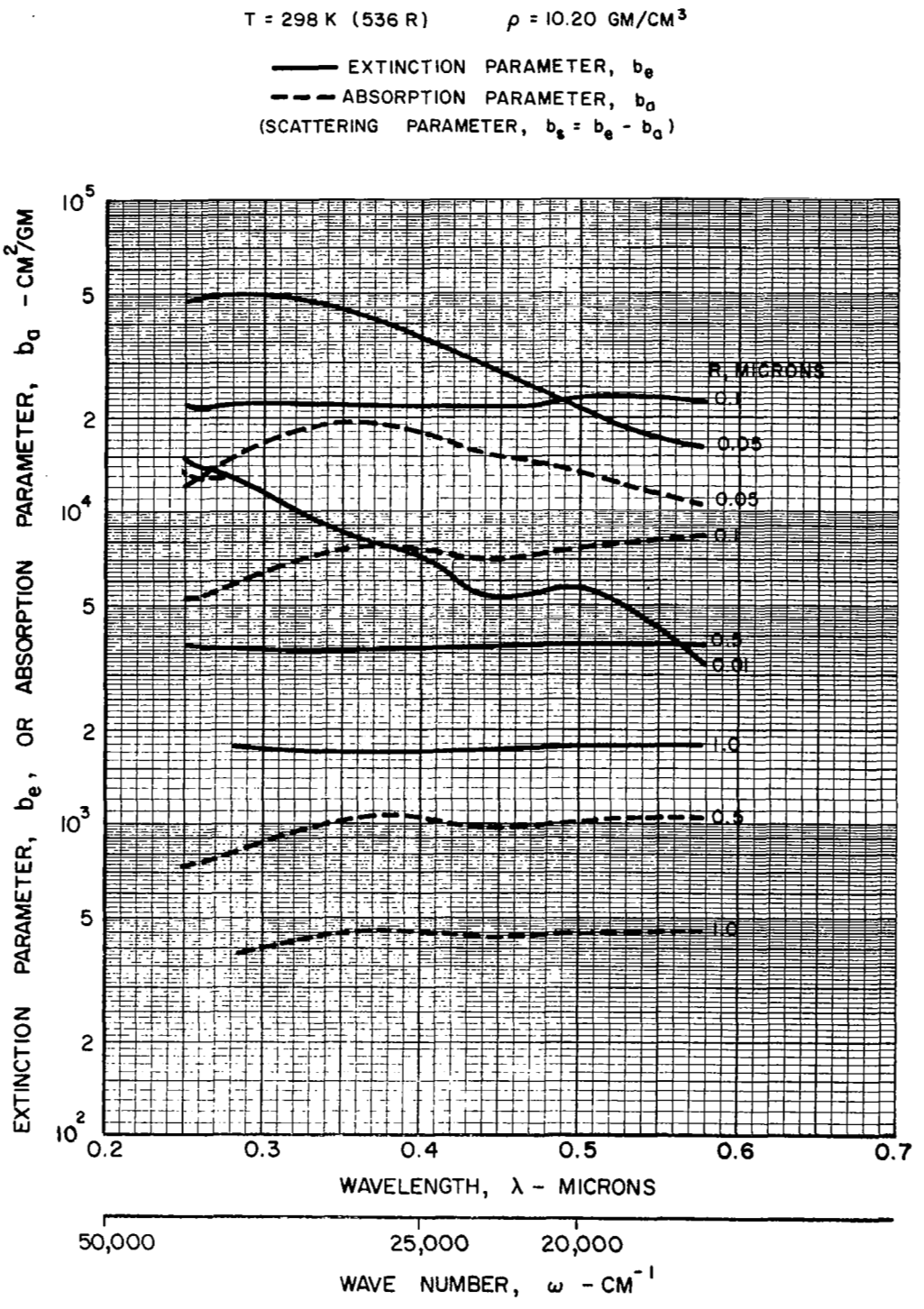

Figure 18

EFFECT OF WAVELENGTH ON THE EXTINCTION AND ABSORPTION PARAMETERS OF SPHERICAL PALLADIUM PARTICLES

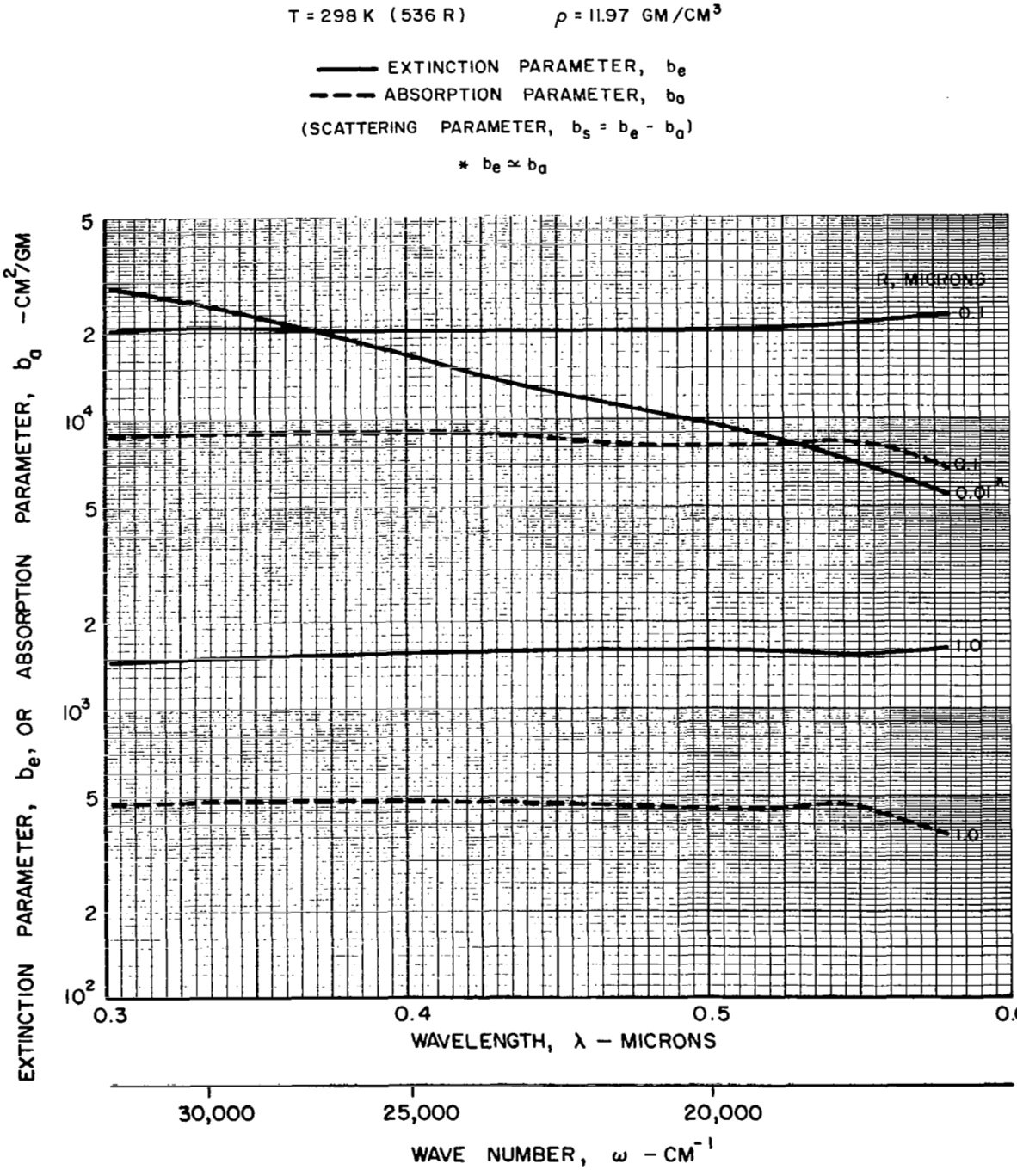

Figure 19

EFFECT OF WAVELENGTH ON THE EXTINCTION AND ABSORPTION PARAMETERS OF SPHERICAL PLATINUM PARTICLES

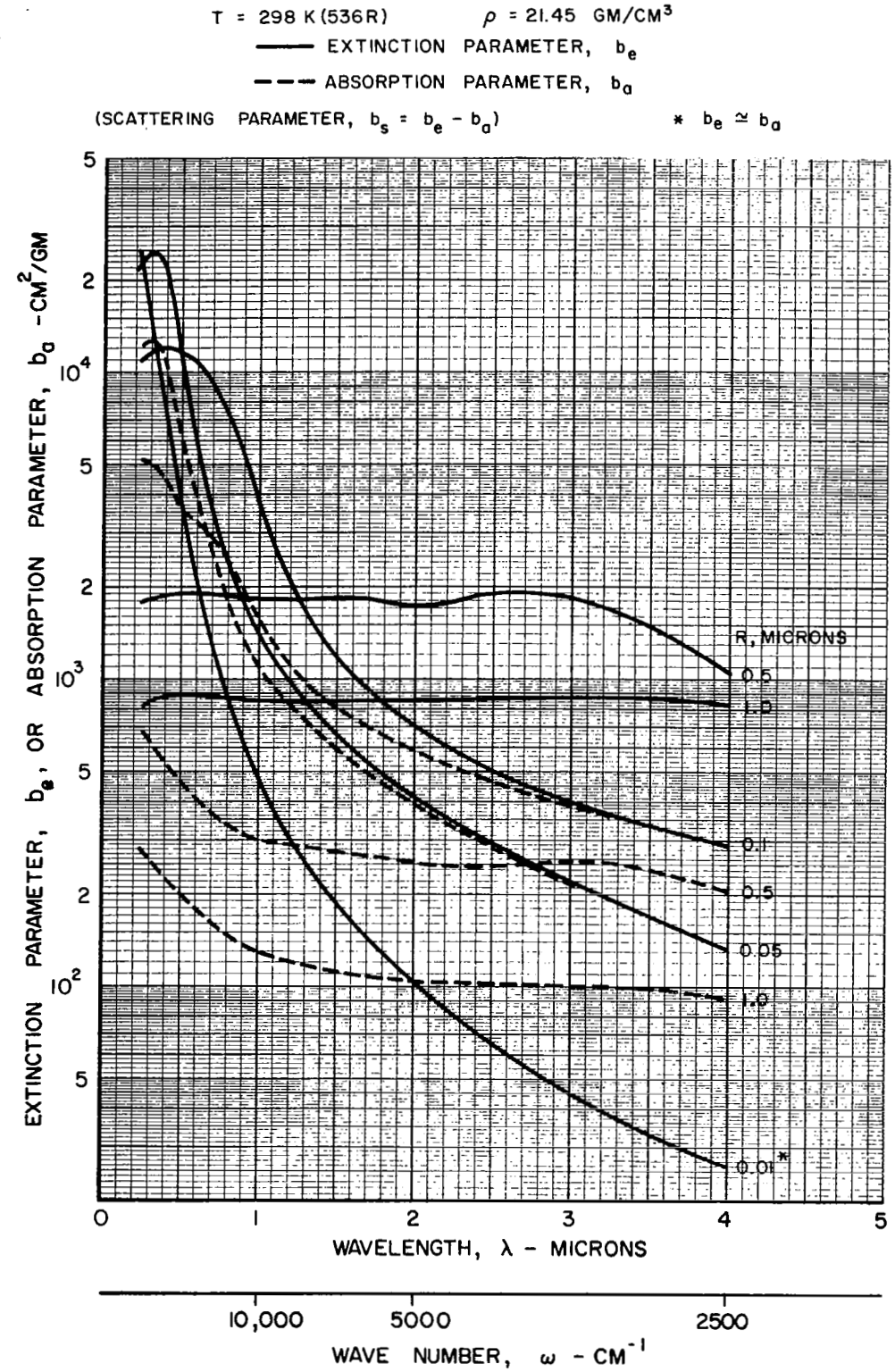

Figure 20

EFFECT OF WAVELENGTH ON THE EXTINCTION AND ABSORPTION PARAMETERS OF SPHERICAL SILICON PARTICLES

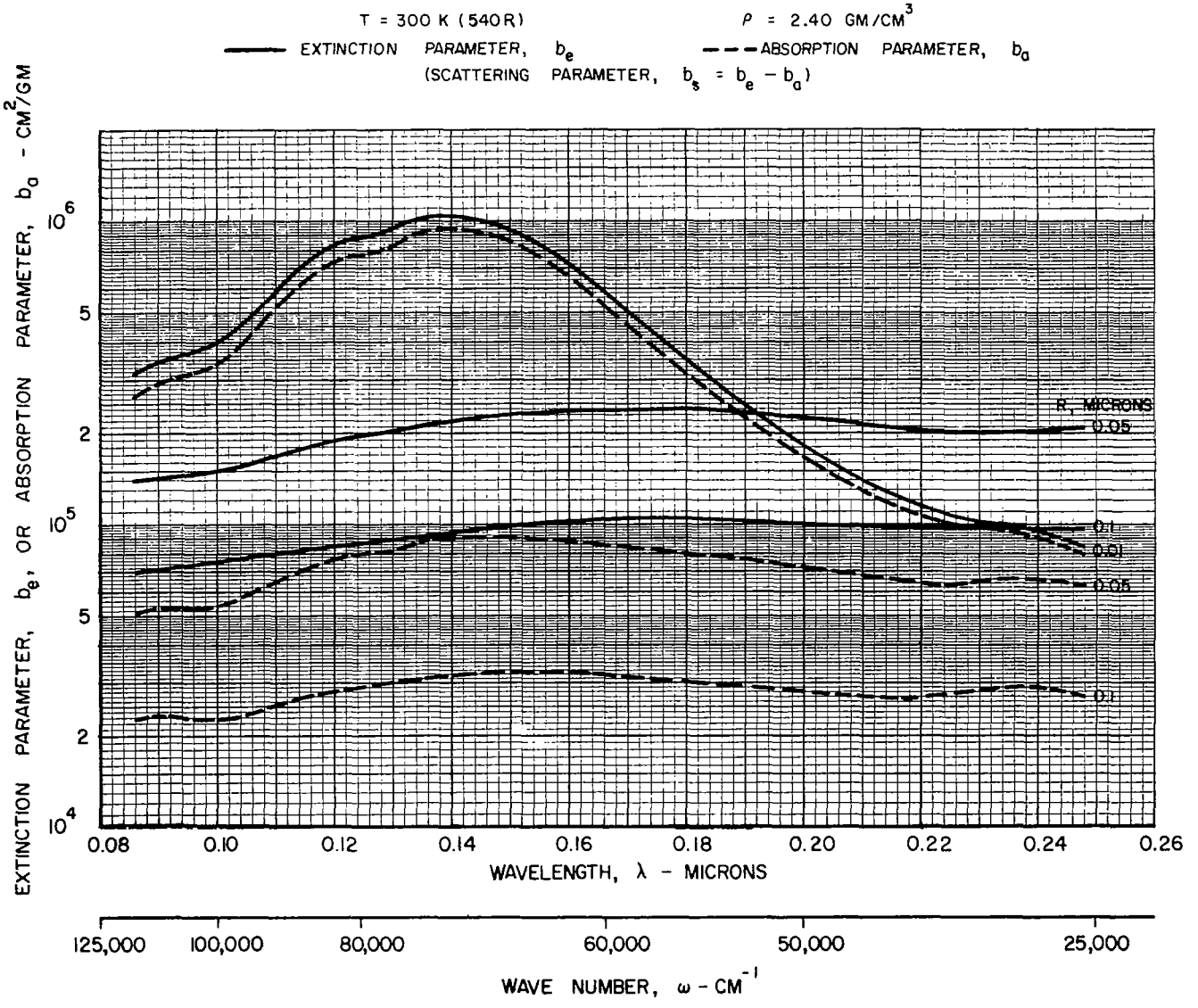

Figure 21

EFFECT OF WAVELENGTH ON THE EXTINCTION AND ABSORPTION PARAMETERS OF SPHERICAL TITANIUM PARTICLES

T = 298 K (536 R) ρ = 4.50 GM/CM^3

– – – ABSORPTION PARAMETER, b_a

——— EXTINCTION PARAMETER, b_e

(SCATTERING PARAMETER, $b_s = b_e - b_a$)

* $b_e \simeq b_a$

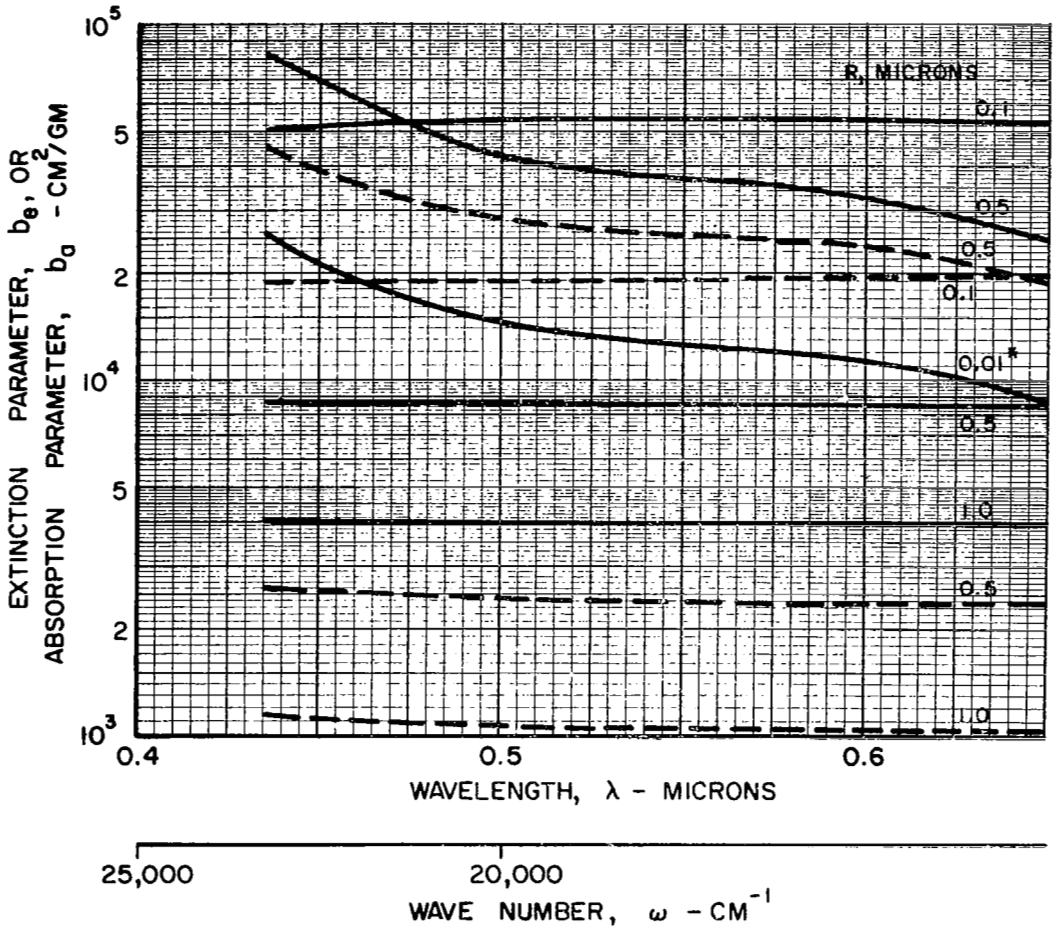

Figure 22

EFFECT OF WAVELENGTH ON THE EXTINCTION AND ABSORPTION PARAMETERS OF SPHERICAL TUNGSTEN PARTICLES

T = 298 (536 R) ρ = 19.30 GM/CM^3

——— EXTINCTION PARAMETER, b_e

— — ABSORPTION PARAMETER, b_a

(SCATTERING PARAMETER, $b_s = b_e - b_a$)

* $b_e \simeq b_a$

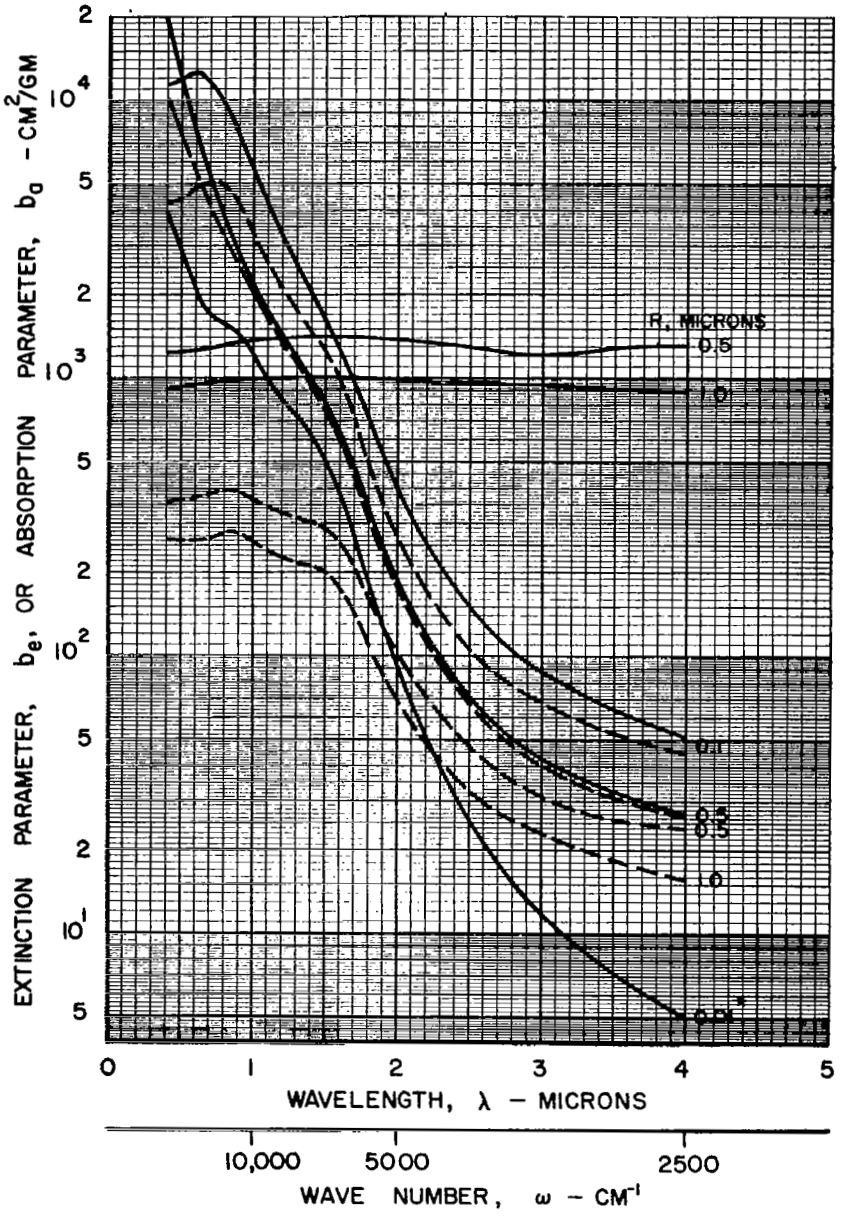

Figure 23

EFFECT OF WAVELENGTH ON THE EXTINCTION AND ABSORPTION PARAMETERS OF SPHERICAL TUNGSTEN PARTICLES

T = 1100 K (1980 R) ρ = 19.30 GM/CM^3

——— EXTINCTION PARAMETER, b_e

– – – ABSORPTION PARAMETER, b_a

(SCATTERING PARAMETER, $b_s = b_e - b_a$)

* $b_e \simeq b_a$

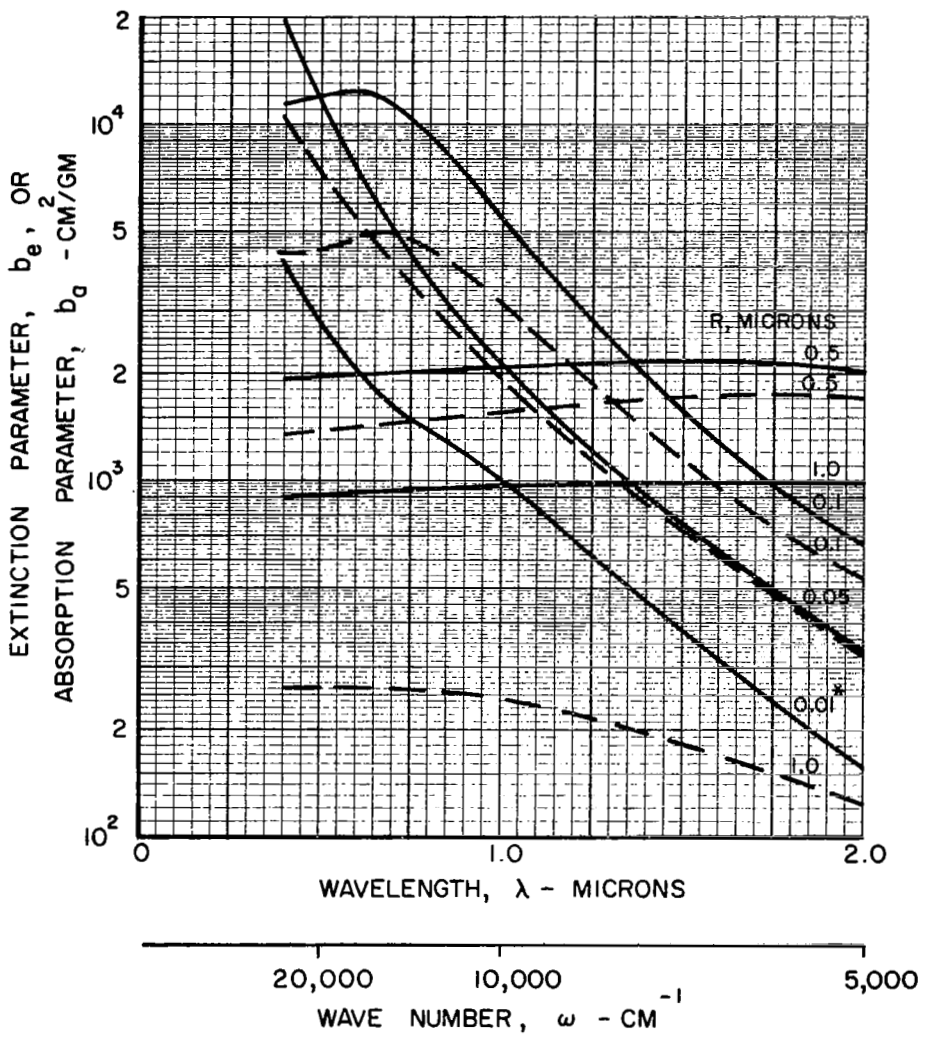

Figure 24

EFFECT OF WAVELENGTH ON THE EXTINCTION AND ABSORPTION PARAMETERS OF SPHERICAL TUNGSTEN PARTICLES

T = 1600 K (2880 R) ρ = 19.30 GM/CM^3

—— EXTINCTION PARAMETER, b_e

– – – ABSORPTION PARAMETER, b_a

(SCATTERING PARAMETER, $b_s = b_e - b_a$) * $b_e \simeq b_a$

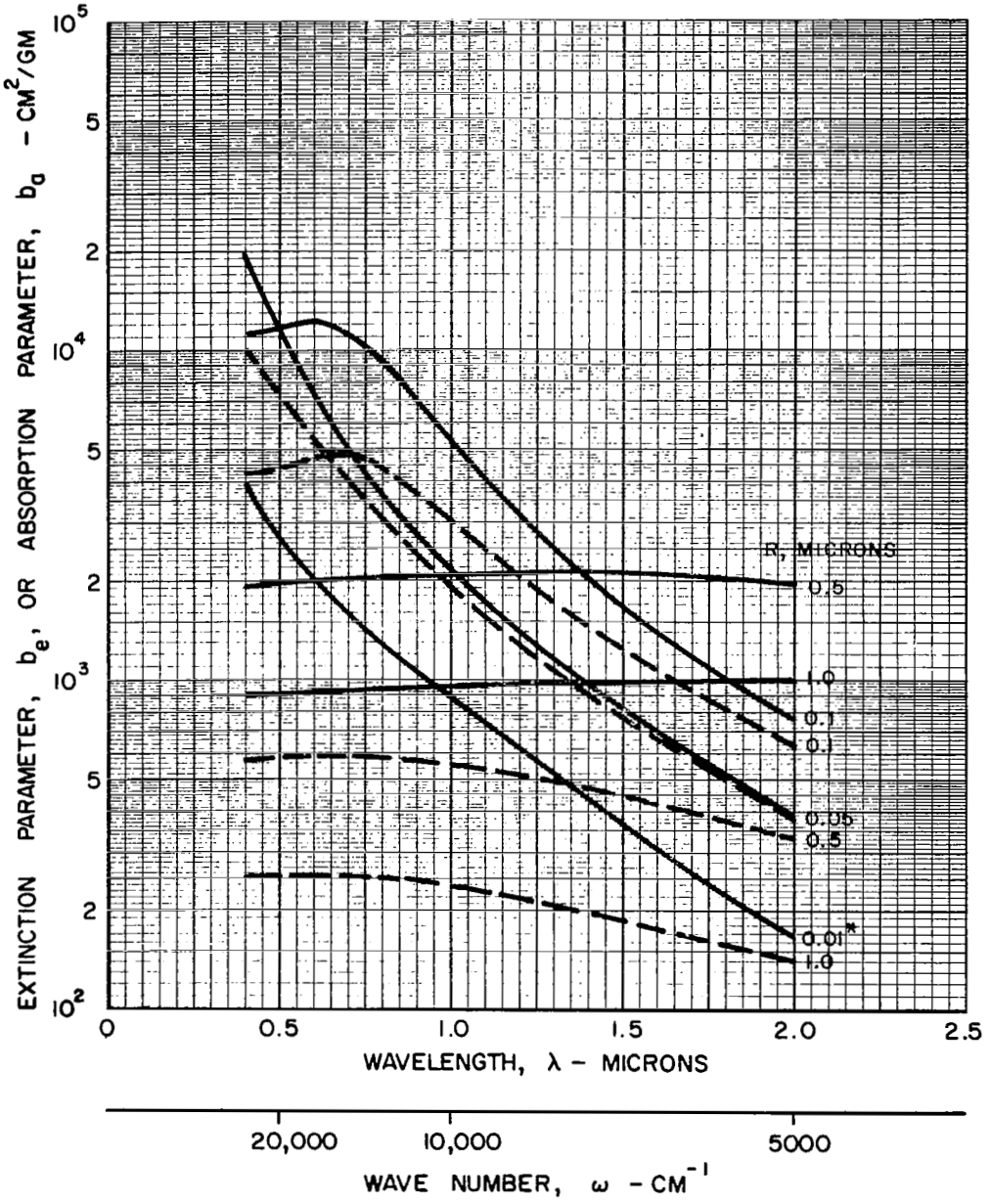

Figure 25

EFFECT OF WAVELENGTH ON THE EXTINCTION AND ABSORPTION CROSS-SECTIONS OF TUNGSTEN

T = 298 K (536 R)

——— EXTINCTION CROSS-SECTION, σ_e

– – – ABSORPTION CROSS-SECTION, σ_a

(SCATTERING CROSS-SECTION, $\sigma_s = \sigma_e - \sigma_a$) * $\sigma_e \simeq \sigma_a$

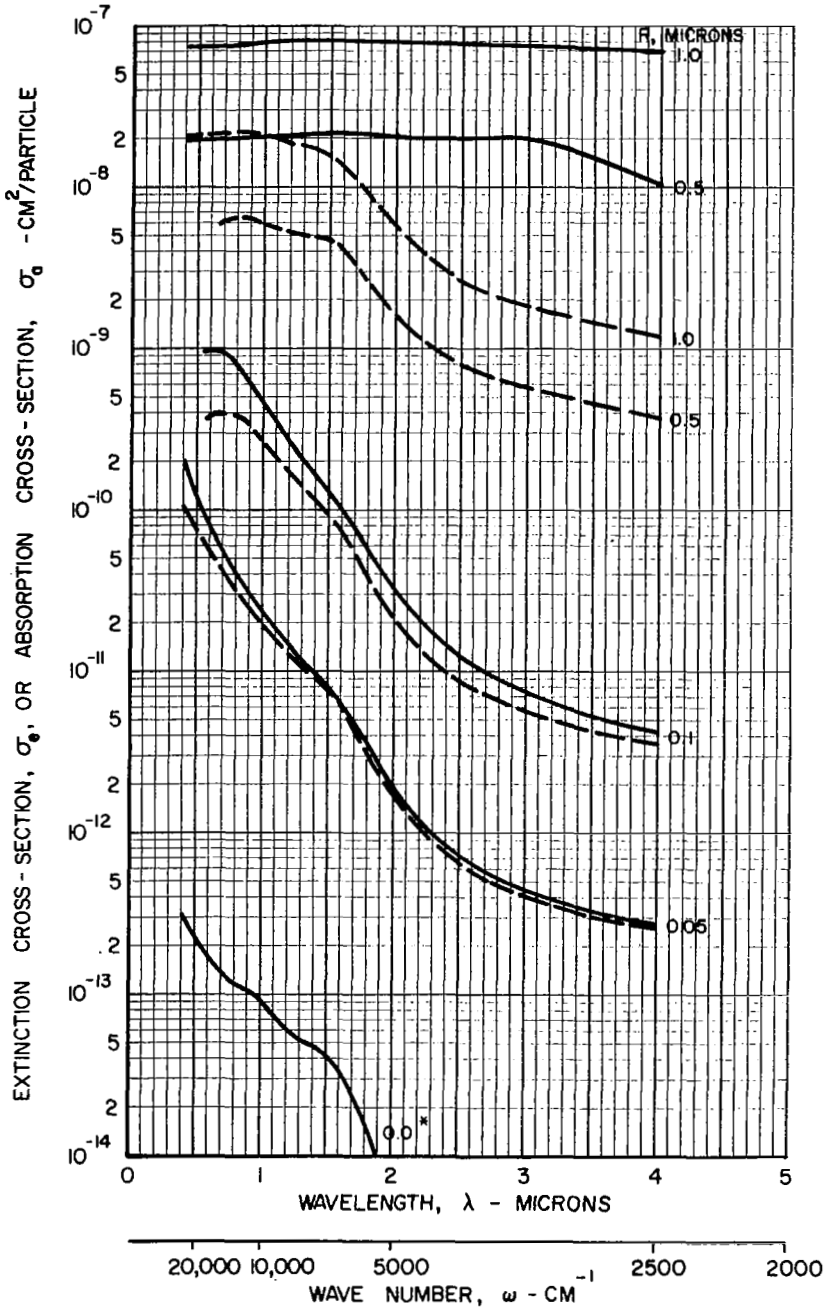

Figure 26

EFFECT OF RADIUS ON THE EXTINCTION AND ABSORPTION PARAMETERS OF SPHERICAL ALUMINUM PARTICLES

T = 298 K (536 R) ρ = 2.70 GM/CM^3

——— EXTINCTION PARAMETER, b_e

– – – ABSORPTION PARAMETER, b_a

(SCATTERING PARAMETER, $b_s = b_e - b_a$)

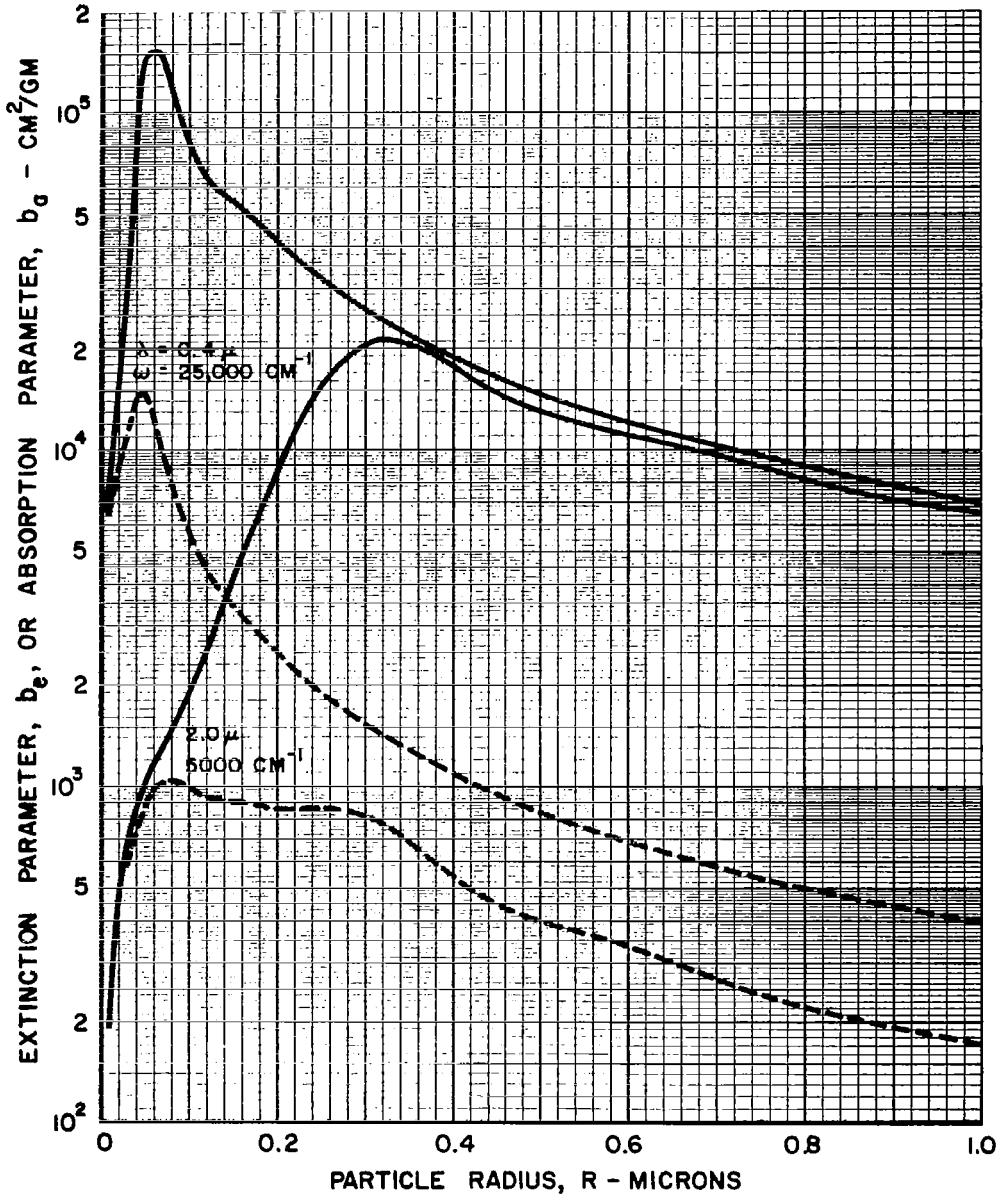

Figure 27

EFFECT OF RADIUS ON THE EXTINCTION AND ABSORPTION PARAMETERS OF SPHERICAL CARBON PARTICLES

T = 2250 K (4050 R) ρ = 2.00 GM/CM^3

——— EXTINCTION PARAMETER, b_e

– – – ABSORPTION PARAMETER, b_a

(SCATTERING PARAMETER, $b_s = b_e - b_a$)

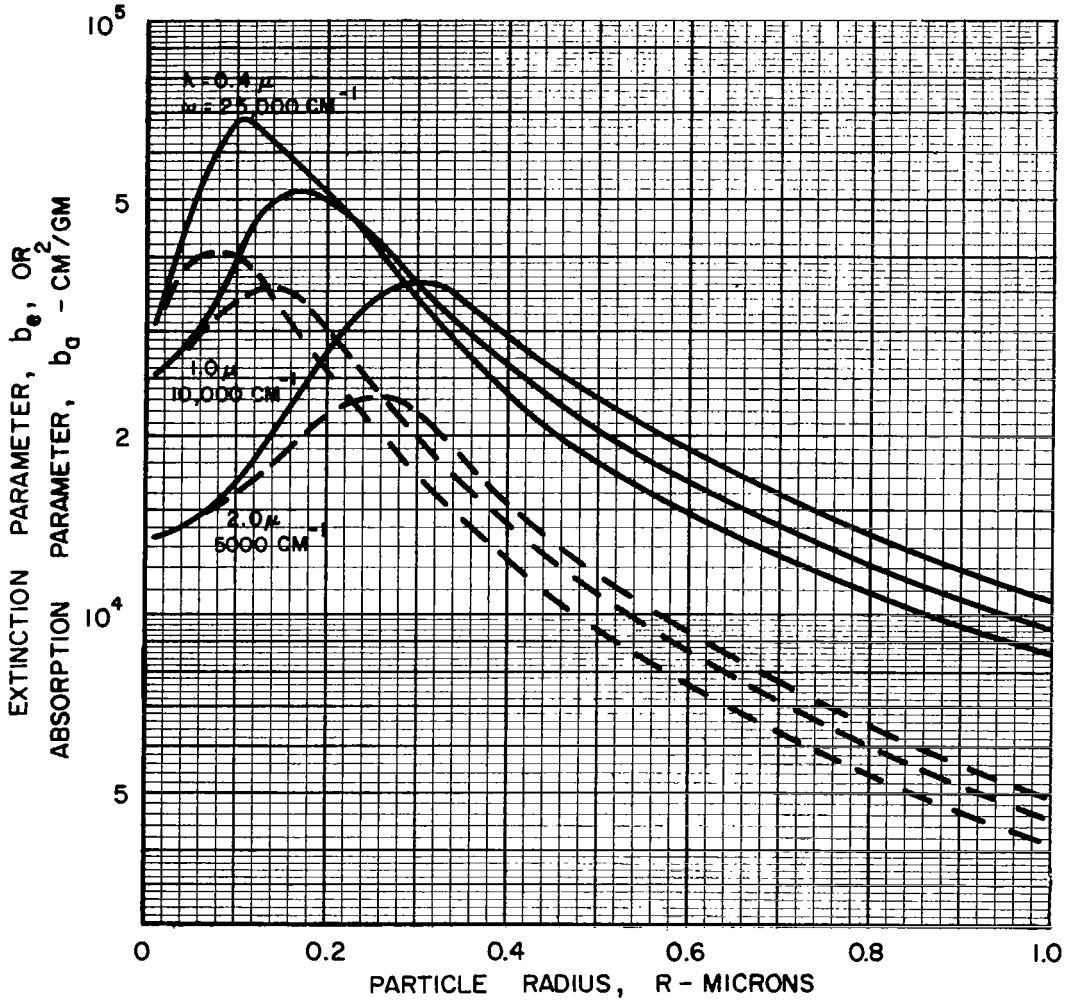

Figure 28

EFFECT OF RADIUS ON THE EXTINCTION AND ABSORPTION PARAMETERS OF SPHERICAL PLATINUM PARTICLES

T = 298 K (536R) ρ = 21.45 GM/CM^3

—— EXTINCTION PARAMETER, b_e

– – – ABSORPTION PARAMETER, b_a

(SCATTERING PARAMETER, $b_s = b_e - b_a$)

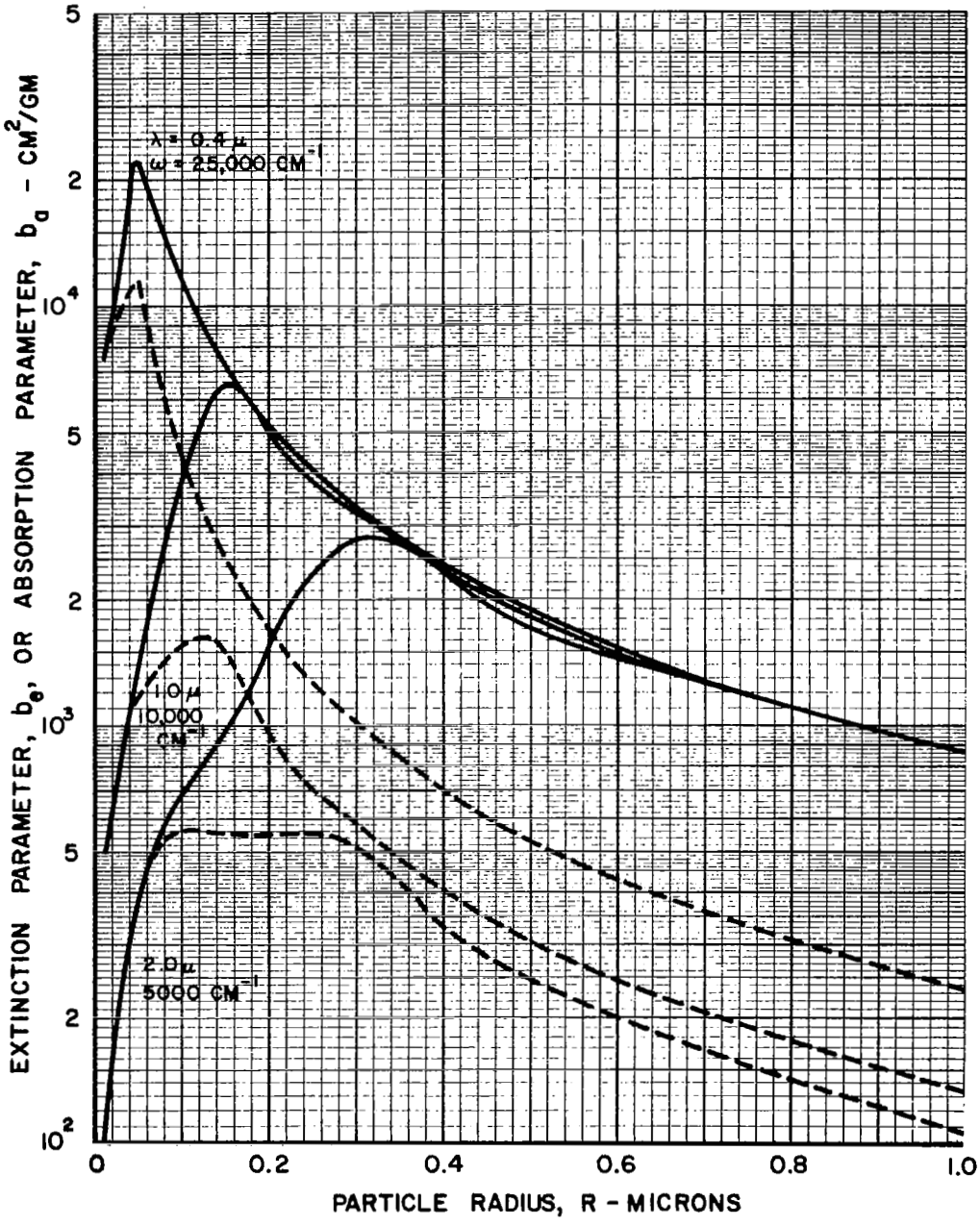

Figure 29

EFFECT OF RADIUS ON THE EXTINCTION AND ABSORPTION PARAMETERS OF SPHERICAL TUNGSTEN PARTICLES

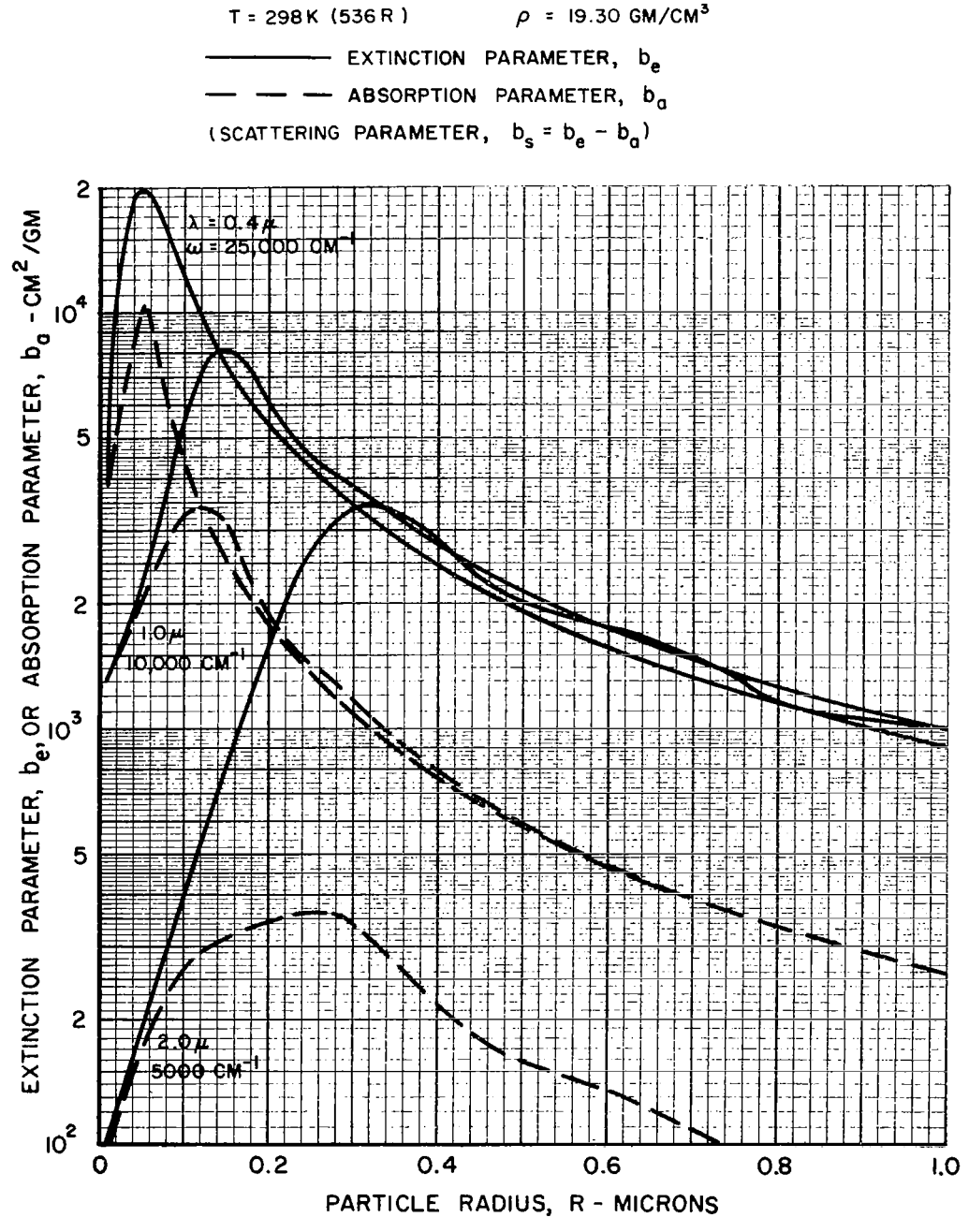

Figure 30

EFFECT OF RADIUS ON THE EXTINCTION AND ABSORPTION PARAMETERS OF SPHERICAL TUNGSTEN PARTICLES

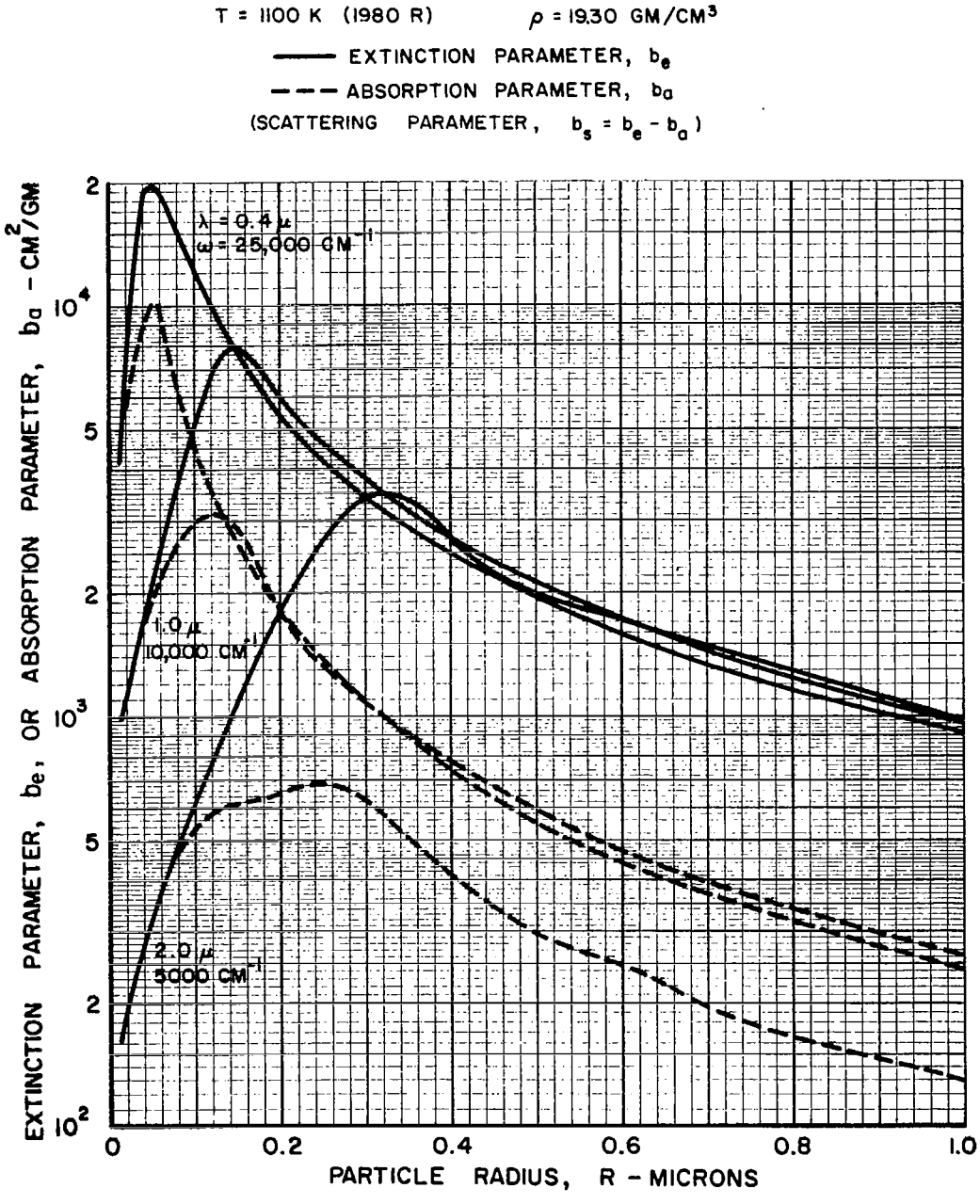

Figure 31

EFFECT OF RADIUS ON THE EXTINCTION AND ABSORPTION PARAMETERS OF SPHERICAL TUNGSTEN PARTICLES

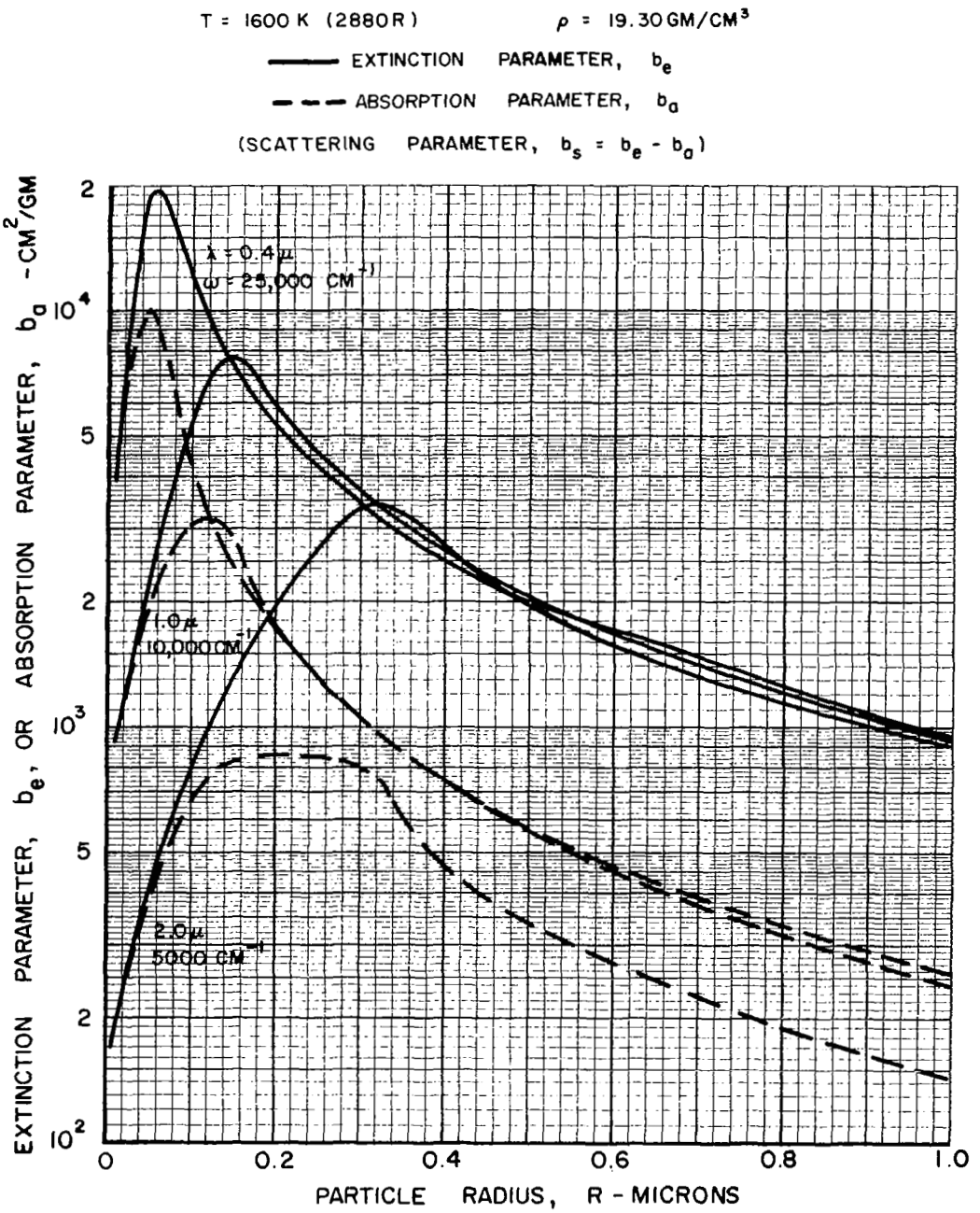

Figure 32

EFFECT OF TEMPERATURE ON THE EXTINCTION AND ABSORPTION PARAMETERS OF SPHERICAL TUNGSTEN PARTICLES

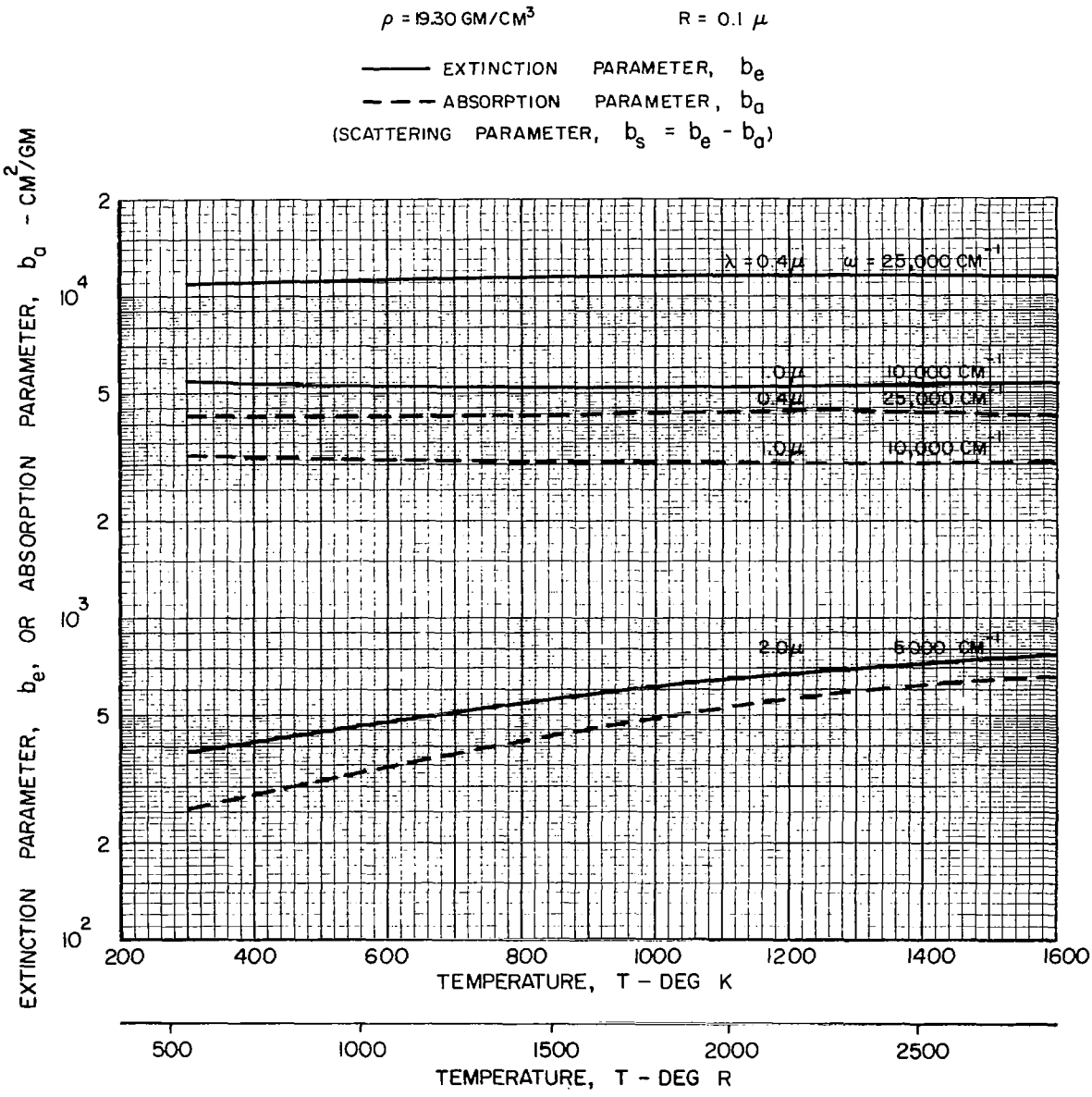

Figure 33

EFFECT OF MELTING-POINT TEMPERATURE ON THE ABSORPTION PARAMETER OF POSSIBLE SEED MATERIALS

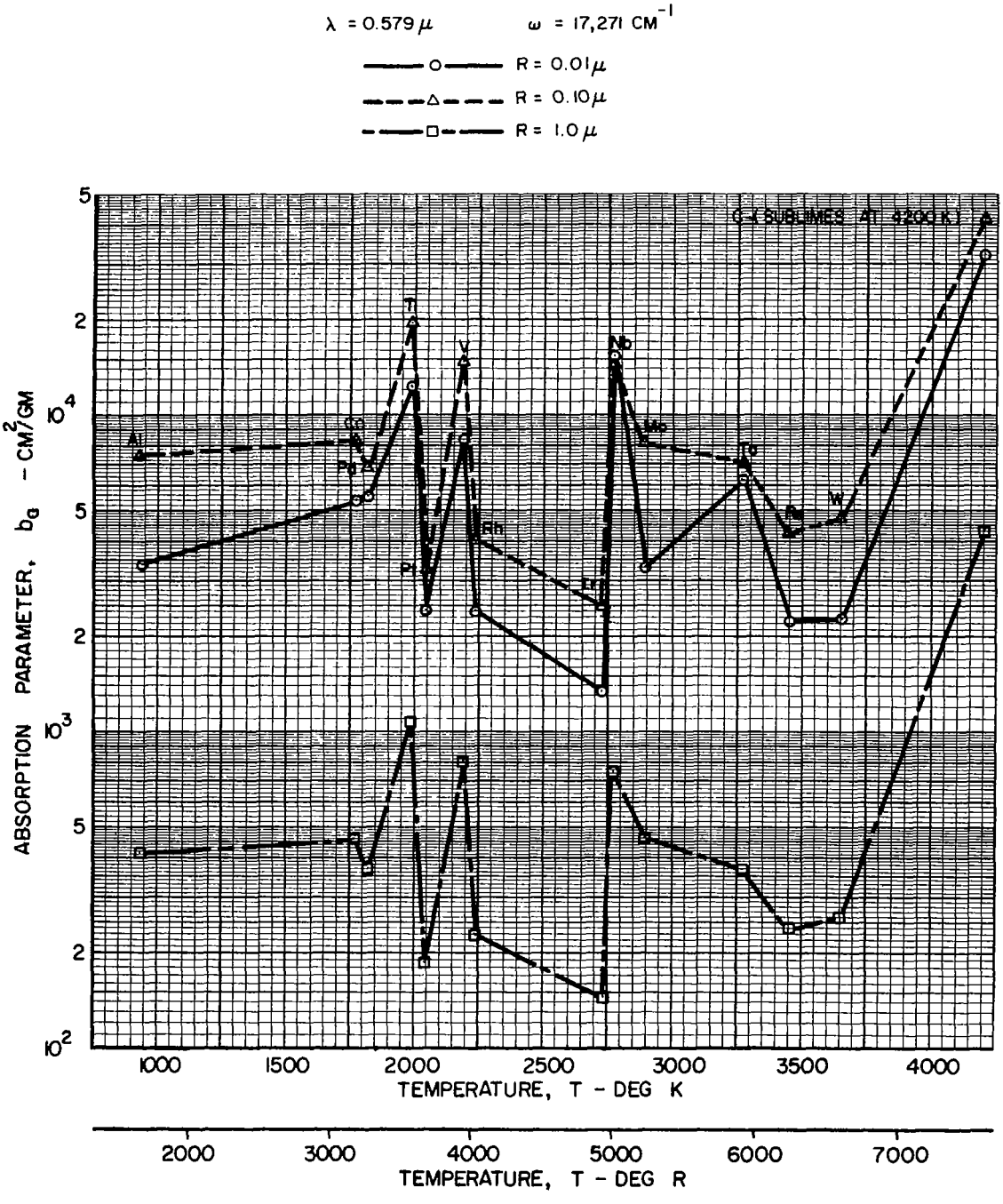

Figure 34

EFFECT OF BOILING-POINT TEMPERATURE ON THE ABSORPTION PARAMETER OF POSSIBLE SEED MATERIALS

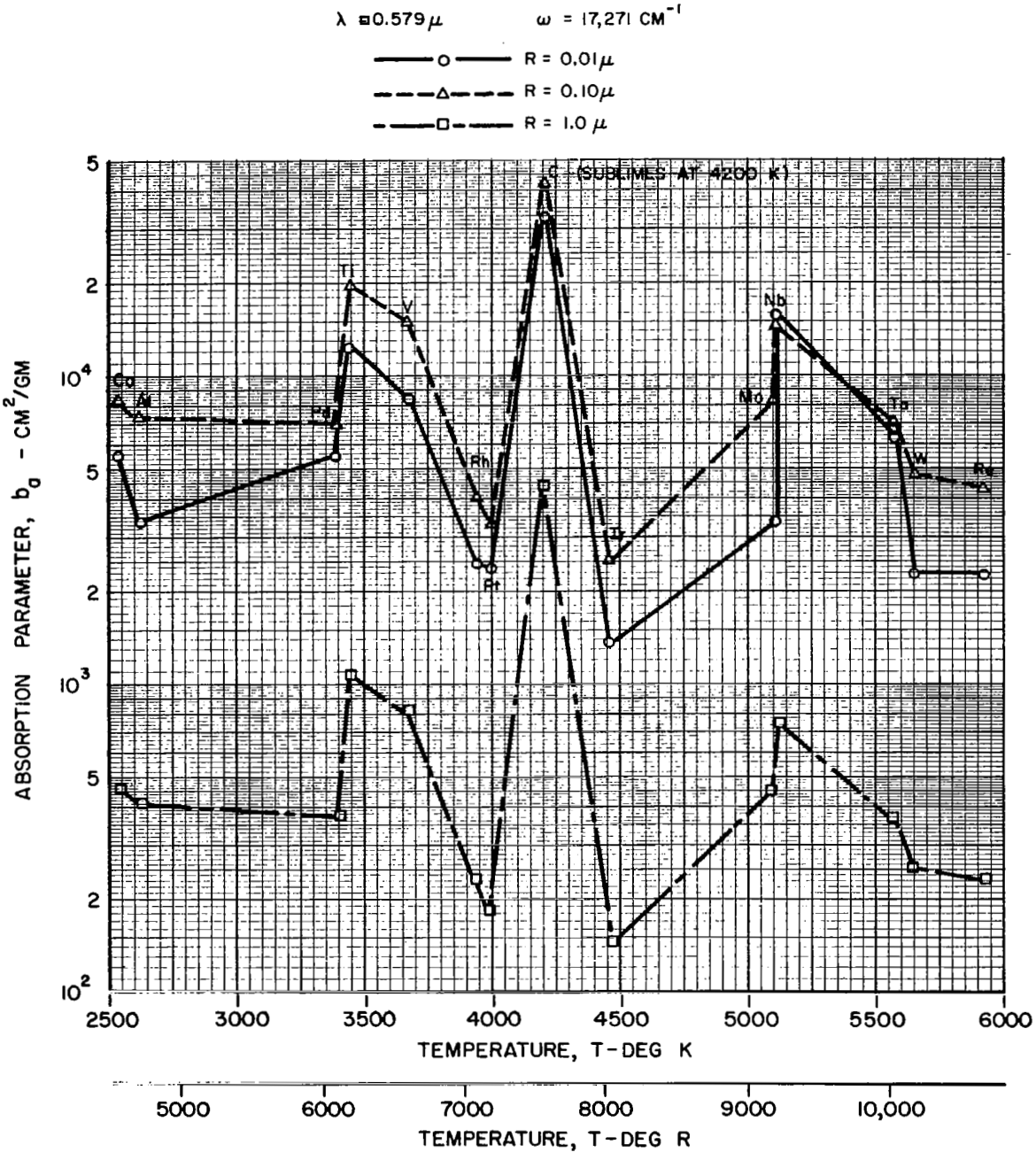

Figure 35

EFFECT OF MASS DENSITY ON THE ABSORPTION PARAMETER OF POSSIBLE SEED MATERIALS

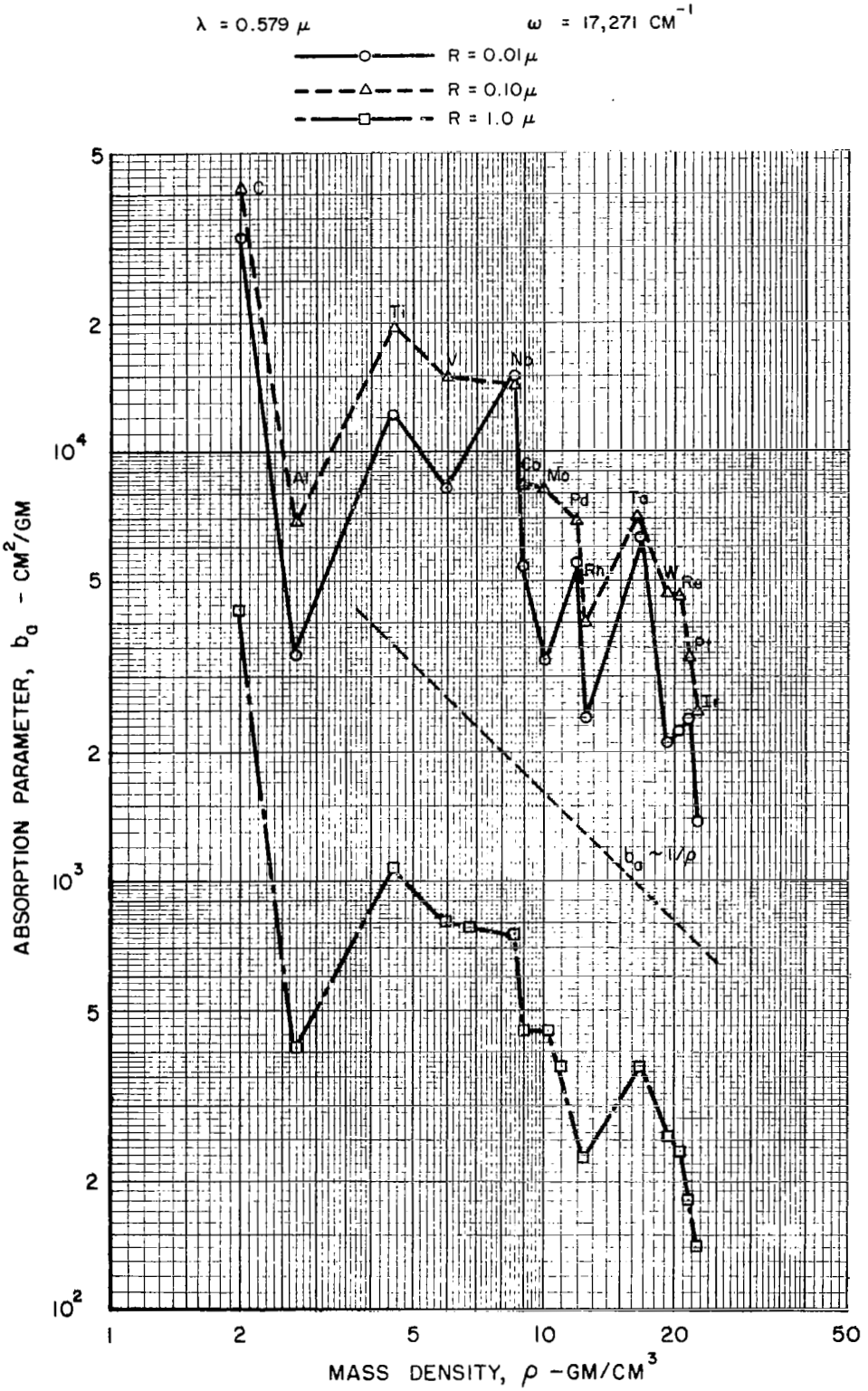

Figure 36

EFFECT OF ATOMIC WEIGHT ON THE ABSORPTION PARAMETER OF POSSIBLE SEED MATERIALS